Food Eng Rev (2014) 6:56–88
DOI 10.1007/s12393-014-9075-x

REVIEW ARTICLE

High-pressure Processing: Kinetic Models for Microbial and Enzyme Inactivation

Vinicio Serment-Moreno · Gustavo Barbosa-Cánovas · José Antonio Torres · Jorge Welti-Chanes

Received: 26 July 2013 / Accepted: 6 February 2014 / Published online: 25 February 2014

Abstract High-pressure processing (HPP) has become the most widely accepted nonthermal food preservation technology. The pressure range for commercial processes is typically around 100–600 MPa, whereas moderate temperature (up to 65 °C) may be used to increase microbial and enzymatic inactivation levels. However, these industrial processing conditions are insufficient to achieve sterilization since much higher pressure levels (>1,000 MPa) would be required to inactivate bacterial endospores and enzymes of importance in food preservation. The next generation of commercial pressure processing units will operate at about 90–120 °C and 600–800 MPa for treatments defined as pressure-assisted thermal processing or pressure-assisted thermal sterilization if the commercial food sterilization level required is achieved. Most published HPP kinetic studies have focused only on pressure effects on the microbial load and enzyme activity in foods and model systems. Published work on primary and secondary models to predict simultaneously the effect of pressure and temperature on microbial and enzymatic inactivation kinetics is still incomplete. Moreover, few references provide a detailed and complete analysis of the theoretical, empirical, and semiempirical kinetic models proposed to predict the level of microbial and enzyme inactivation achieved. This review organizes these published kinetic models according to the approach used and then presents an in-depth and critical revision to define the modeling research needed to provide commercial users with the computational tools needed to develop and optimize pasteurization and sterilization pressure treatments.

Keywords High-pressure processing · Pressure-assisted thermal processing · Primary and secondary models · Kinetics · Enzyme inactivation · Microbial inactivation

V. Serment-Moreno · J. Welti-Chanes (✉)
Centro de Biotecnología FEMSA, Escuela de Biotecnología y Alimentos, Tecnológico de Monterrey, Av. Eugenio Garza Sada 2501 Sur, Col. Tecnológico, 64849 Monterrey, NL, Mexico
e-mail: jwelti@itesm.com

V. Serment-Moreno
e-mail: vsermentm@gmail.com

G. Barbosa-Cánovas
Center for Nonthermal Processing of Food, Washington State University, Pullman, WA 99164-6120, USA
e-mail: barbosa@wsu.edu
URL: http://www.bsyse.wsu.edu/barbosa

J. A. Torres (✉)
Food Process Engineering Group, Department of Food Science and Technology, Oregon State University, 100 Wiegand Hall, Corvallis, OR 97331, USA
e-mail: J_Antonio.Torres@OregonState.edu

List of symbols

A	Enzyme activity (mg^{-1}, ml^{-1})
A_f	Accuracy factor
a	Linear temperature dependence of the activation volume under isobaric conditions, Eyring–Arrhenius secondary model ($cm^3\ mol^{-1}\ K^{-1}$)
a_w	Water activity
A_0	Enzyme activity prior to thermal or pressure treatments (mg^{-1}, ml^{-1})
A_∞	Residual enzyme activity after long thermal or pressure treatments (mg^{-1}, ml^{-1})
b	Slope parameter, Weibull kinetic model (min^{-n})
b'	Slope parameter, Weibull kinetic model (min^{-1})

c_i; i = 1, 2,…,n	Empirical kinetic model coefficients
C	Concentration, microbial population, or enzyme activity
C_P	Specific heat capacity under isobaric conditions (J mol^{-1} K^{-1})
C_0	Initial concentration, microbial population, or enzyme activity prior to thermal or pressure treatments
C_∞	Final concentration, microbial population, or enzyme activity after long thermal or pressure treatments
D_T	Decimal reduction time describing the lethal thermal effect assuming first-order kinetics (s, min)
D_P	Decimal reduction time describing the lethal pressure effect assuming first-order kinetics (s, min)
D_{Pref}	Decimal reduction time describing the lethal pressure effect at a reference pressure and assuming first-order kinetics (s, min)
E_a	Arrhenius activation energy describing the temperature dependence of a process kinetics (J mol^{-1} K^{-1})
E_{aP}	Arrhenius activation energy at a reference pressure (J mol^{-1} K^{-1})
$F(t)$	System failure time predicted with the Weibull distribution function (s, min)
f_P	Slope parameter when pressure is the independent Weibull kinetic model variable (MPa^{-n})
f_T	Slope parameter when temperature is the independent Weibull kinetic model variable (MPa^{-n})
g	Activation energy exponential pressure dependence under isothermal conditions, Eyring–Arrhenius secondary model (MPa^{-1})
G	Gibbs free energy (J mol^{-1})
ΔG	Gibbs free energy change (J mol^{-1})
ΔG_{ref}	Gibbs free energy change at reference pressure and temperature conditions (J mol^{-1})
h	Planck constant (6.6260×10^{-34} J s)
H	Difference between the upper and lower asymptote, log-logistic kinetic model
HPP	High-pressure processing
k	Reaction rate constant (min^{-1})
k_B	Boltzmann constant (1.3806×10^{-23} J K^{-1})
k_{refP}	Reaction rate constant at a reference pressure (min^{-1})
k_{refT}	Reaction rate constant at a reference temperature (min^{-1})
$k^{\neq}$	Activated complex reaction rate constant (min^{-1})
K	Equilibrium constant for a reaction
$K^{\neq}$	Pseudo-equilibrium constant for a reactant to activated complex formation
L	Lethality (cfu s^{-1}, cfu min^{-1})
m	Exponent, Weibull log-logistic secondary model
n	Exponent, Weibull kinetic model
N	Microbial population (cfu g^{-1}, cfu ml^{-1})
N_0	Microbial population prior to thermal or pressure treatments (cfu g^{-1}, cfu ml^{-1})
N_∞	Microbial population surviving long thermal or high-pressure treatments (cfu g^{-1}, cfu ml^{-1})
p	Scale parameter, Weibull distribution function
P	Pressure (MPa)
P_c	Critical pressure parameter, Weibull log-logistic secondary model (MPa)
P_{c0}	Critical pressure parameter at a reference temperature, Weibull exponential secondary model (MPa)
P_{ref}	Reference pressure (MPa)
PATP	Pressure-assisted thermal processing
PATS	Pressure-assisted thermal sterilization
q	Shape parameter, Weibull distribution function
r	Chemical reaction rate
R	Ideal gas constant (8.314 J mol^{-1} K^{-1}, 8.30865 cm^3 MPa mol^{-1} K^{-1})
R^2	Regression coefficient
ΔS	Entropy change, thermodynamic model (J mol^{-1} K^{-1})
ΔS_{ref}	Entropy change at a reference temperature, thermodynamic model (J mol^{-1} K^{-1})
t	Time (s, min)
T	Temperature (K)
T_c	Critical temperature parameter, Weibull log-logistic secondary model (K)
T_{c0}	Critical temperature parameter at a reference temperature, Weibull exponential secondary model (K)
T_{ref}	Reference temperature (K)
$\overline{V}_P$	Partial molar volume of products in a chemical reaction (cm^3 mol^{-1})
$\overline{V}_R$	Partial molar volume of reactants in a chemical reaction (cm^3 mol^{-1})
$\overline{V}^{\neq}$	Partial molar volume of the active complex, transitional state theory (cm^3 mol^{-1})
$\overline{V}_T^{\neq}$	Partial molar volume of the active complex at a reference temperature, transitional state theory (cm^3 mol^{-1})

$\Delta\overline{V}_{reaction}$ Molar volume change of a chemical reaction ($cm^3\ mol^{-1}$)

$\Delta\tilde{V}^{\neq}$ Molar volume change to reach the active complex, transitional state theory

w_P Exponential pressure dependence of parameter b', Weibull secondary model (MPa^{-1})

w_T Exponential temperature dependence of parameter b', Weibull secondary model (K^{-1})

z_P Pressure-resistant parameter under isothermal conditions, Bigelow model (MPa)

z_T Thermal-resistant parameter under isobaric conditions, Bigelow model (K)

Greek symbols

α Thermal expansivity coefficient, thermodynamic model ($cm^3\ mol^{-1}\ K^{-1}$; upper asymptote, log-logistic kinetic model)

$\Delta\alpha$ Thermal expansivity coefficient change under nonisothermal and isobaric conditions ($cm^3\ mol^{-1}\ K^{-1}$)

β Compressibility factor, thermodynamic model ($cm^6\ J^{-1}\ mol^{-1}$; lower asymptote, log-logistic kinetics model)

$\Delta\beta$ Compressibility factor change under nonisothermal and isobaric conditions, thermodynamic model ($cm^6\ J^{-1}\ mol^{-1}$)

Ψ Log fraction parameter, Weibull biphasic kinetic model

Ω Maximum inactivation rate, log-logistic kinetic model (cfu s^{-1}, cfu min^{-1})

τ Log time at which the maximum inactivation rate starts, log-logistic kinetic model (min)

λ Time interval in which no high-pressure processing inactivation occurs, secondary quasi-chemical kinetic model (min)

$\upsilon^{\neq}$ Frequency at which the activated complex transforms into products, energy distribution described by the Planck equation (s^{-1})

Introduction

Food Safety and High-Pressure Processing (HPP)

High-pressure processing (HPP) has successfully evolved into one of the most recurrent alternatives to thermal food processing. In the last 20 years, the number of HPP installations in the world, and processing a wide variety of foods, grew from one in 1990 to nearly 200 units with a concurrent tenfold increase in size from 25 to 50 L to 300–500 L [7, 74]. In addition, the operating pressure level increased from about 400 MPa to about 600–800 MPa reducing pressure holding times from 15 to 30 min to a few minutes. The rapidly growing number of installed units with shorter processing time and larger vessel volume has dramatically increased the installed pressure processing capacity. The high consumer acceptance of HPP treatments reflects, in most cases, a minimal alteration of the original nutritional and sensory food characteristics while effectively inactivating pathogens, spoilage microorganisms, and enzymes [5, 24, 59, 122].

Microbial Inactivation

Microorganisms are affected by several simultaneous lethal effects with cellular membrane damage frequently reported as a dominant factor [68, 81, 82, 117]. Acyl chains of the phospholipid bilayer may experience crystallization, leading to bud formation, membrane rupture, and intracellular material leakage [68, 81]. Low-pressure treatment levels ranging from 20 to 180 MPa result usually in sublethal cellular damage. Microbial inactivation of a large variety of pathogenic and spoilage bacteria vegetative forms is achieved above 200–400 MPa, when irreversible protein/enzyme denaturation and intracellular content leakage occur [57, 74]. On the other hand, HPP alone cannot inactivate bacterial spores as they can withstand pressures over 1,000 MPa when temperature after compression is below 70–80 °C [68, 74, 82, 96, 106].

Enzyme Inactivation

Protein denaturation effects vary depending on the protein structure and external factors such as pressure level, temperature, pH, and solvent composition [78, 125]. Irreversible changes may include dissociation of oligomeric proteins into their subunits, conformational changes of the substrate/active site, and aggregation or gelation of proteins due to a decrease in the solution volume or the association of hydrophobic molecules [44, 78, 125]. Reversible protein modifications are typically observed in the 100–300 MPa range [123] but enzyme activity may also be enhanced within this range [33, 78, 125]. Some enzymes can display high baroresistance, and pressures over 500 MPa combined with moderate temperatures are required to induce significant inactivation.

Current Status of High-pressure Processing

Commercial HPP units operate typically within a 100–600 MPa range and temperatures between 5–65 °C [3, 7, 74]. Since these mild conditions are insufficient to achieve bacterial spore inactivation, units operating at

higher pressure (600–800 MPa) and elevated temperature (90–120 °C) will be necessary [93, 108]. This novel procedure, known as pressure-assisted thermal processing (PATP) or pressure-assisted thermal sterilization (PATS) if bacterial spore inactivation attaining commercial food sterility is achieved, is under development. However, at PATP temperature and pressure conditions, significant chemical changes cannot be ignored due to their potential for the breaking of covalent bonds [107, 108]. Approval has been granted by the US Food and Drug Administration for the commercial production of low-acid foods using PATS. Mashed potatoes inoculated with *Clostridium botulinum* spores were subjected to a shelf-life study under the severe conditions used when testing food supplies for the United States Army. No microbial growth was observed during storage, and the sensory quality observed was superior to those possible with a conventional thermal process [75].

Unlike other physical and chemical factors, pressure is delivered uniformly throughout the vessel almost immediately after being applied [95]. As a result of this compression, the food temperature increases depending on factors such as food composition, pressure level, initial food and pressurizing media temperature, pressurization media used, vessel loading factor, and equipment design. The rise in temperature per 100 MPa due to adiabatic compression heating has been reported to be $\approx$3 °C for water and $\approx$8–9 °C for fat and oils, while proteins and carbohydrates show intermediate values [3, 77, 80]. The prediction of the temperature rise remains an area of active research.

In spite of the PATP/PATS process already approved by the FDA and suggesting the upcoming commercialization of this technology, extensive databases of predictive models, kinetic parameters, and standardized procedures similar to those developed for conventional technologies such as thermal processing are not yet available. At present, most of the kinetics information on high-pressure processing of foods is disperse and obtained using relatively narrow ranges for the experimental pressure–temperature conditions tested. Even though the scientific data obtained may be sufficient for the development of a food product, it is certainly limited to evaluate the inactivation kinetics models proposed. Analysis of the fit to experimental data is frequently limited to comparing a few models. This review shows that many food scientists are still relying on linear inactivation kinetics, even though concave and sigmoidal trends are frequently observed in pressure treatments. Additionally, most of the reported HPP investigations on inactivation kinetics have focused on pressure effects and often do not take into account the contribution of the temperature changes due to compression of the food and pressurizing fluid, and the heat exchanges involving the product and pressurization media, the vessel walls, and the equipment surroundings. When accurate temperature profiles of HPP are available, inactivation kinetics models should be paired with transport phenomena equations predicting the pressure–temperature profiles under PATP/PATS conditions when analyzing chemical reactions and the inactivation of microorganisms and enzymes in foods. Therefore, the following sections review chemical and biochemical models to provide a concise, analytical reference for high-pressure food processing kinetic models with theoretical, empirical, and semiempirical backgrounds.

Primary Models

Primary modeling consists of developing mathematical expressions based on theoretical principles, empirical observations, or the combination of both, to predict changes in microbial counts, enzyme activity, or chemical concentrations as a function of the processing time. According to the shape of the kinetic behavior predicted, primary models are classified as linear, concave, or sigmoidal.

Linear Primary Models

First-Order Kinetics Model

First-order kinetics continues to be the most often model to describe microbial and enzyme inactivation, although poor estimates can be expected since nonlinear trends are often observed experimentally [23, 86, 89, 124]. It assumes that the change in chemical changes, microbial population, or enzyme activity is directly proportional to their concentration denoted as C in Eq. 1 and described by an inactivation rate constant under constant isobaric and isothermal conditions (k [=] min^{-1}).

$$-\frac{\mathrm{d}C}{\mathrm{d}t} = k \cdot C \tag{1}$$

By integrating from $t = 0$ through treatment time t and from $C\ (t = 0) = C_0$ through $C(t) = C$, the resultant model (Eq. 2) establishes that the Napierian logarithm of C/C_0 will result in a decreasing straight line that goes through the origin.

$$\ln\frac{C}{C_0} = -k \cdot t \tag{2}$$

Microbiologists frequently transform the Napierian logarithm base of Eq. 2 to decimal logarithms and report the number of decimal reductions in the microbial population (Eq. 3).

$$\log_{10}\frac{N}{N_0} = -\frac{k}{2.303} \cdot t \tag{3}$$

Therefore, a decimal reduction time (D_T) can be defined as the time required at a constant lethal temperature T for a tenfold reduction in the microbial load ($\log_{10} N/N_0 = \log 0.1\ N_0/N_0 = -1$) [71, 105]. A similar parameter (D_P) can be defined for the effect of the lethal pressure P [6, 79]. D_P can be calculated as the negative inverse of the $\log_{10}$ linear model slope (Eq. 4).

$$\log_{10}\frac{N}{N_0} = -\frac{1}{D_P}\cdot t \tag{4}$$

The parameter D_P varies (0.01–4 min) depending on the pressure level, the microorganism, and the interaction of intrinsic food product factors with the microorganism (Table 1). For example, *Listeria monocytogenes* has a high-pressure resistance in milk ($D_P = 2.43$–10.99 min) and a much lower in acid media such as orange juice ($D_P = 0.87$–2.87 min). Bacterial spores can show great pressure resistance, but may be readily inactivated ($D_P = 0.1$–0.6 min) with a combination of temperatures above 100 °C and pressures over 400 MPa (Table 1).

Fractional Conversion and Multiphasic Models

The fractional conversion model, a variation of the first-order kinetics model, is obtained by assuming that the thermal or pressure treatment leaves a residual enzyme activity or microbial load with much higher inactivation resistance. Thus, Eq. 1 is integrated from its initial conditions ($C_0 = N_0 = A_0$; at $t = 0$) to its final conditions where the remaining microbial population or enzyme activity after a prolonged treatment time is C_∞ ($t = \infty$), yielding the fraction conversion model (Eq. 5) [34, 66, 90, 112].

$$C = C_\infty + (C_0 - C_\infty)\cdot\exp(-k\cdot t) \tag{5}$$

A similar approach was followed to develop the multiphasic model, for which populations with different resistance toward the pasteurization or sterilization treatment are represented by the presence of two or more isoenzymes or microbial subpopulations [14, 34, 86]. The simplest form of the multiphasic model considers the presence of a labile fraction (C_L) that is inactivated more rapidly and a stable fraction (C_S) able to withstand longer treatment times. Each fraction is inactivated at a distinct rate, and the concentration (C) observed represents the sum of C_L and C_S at any given time. By separating Eq. 1 into the labile and stable fractions, and by solving the integral, this form of the multiphasic model can be described by Eq. 6.

$$C = C_L\cdot\exp(-k_L\cdot t) + C_S\exp(-k_S\cdot t) \tag{6}$$

Campanella and Peleg [12] reported major drawbacks of biphasic models. First and probably most importantly, changes in the kinetic rate constant may occur as a result of alterations in the food matrix rather than caused by populations with different pressure and/or temperature resistance. These authors questioned also the lack of generality of the model and considered it to be too specific. Peleg [86] suggested that if enzymatic and microbial subpopulations differing in inactivation resistance do exist, they should be isolated to perform independent inactivation kinetics to validate the multiphasic model.

Concave Primary Models

Weibull Model

Many models have been developed as alternatives to linear inactivation kinetics [111]. Both mechanistic and empirical equations have led to an adequate fit to experimental data, but often they are too specific and/or complex [67]. Several authors have considered the approach of treating inactivation as the distribution of the survival microbial population/enzyme activity associated with diverse factors such as differences in the treatment intensity or due to an heterogeneous resistance [67, 86, 110].The Weibull distribution (Eq. 7) is used in engineering science to predict the time of failure $F(t)$ of an electronic or mechanical system [110]. Thus, the residual microbial/enzyme activity curve can be interpreted as a cumulative function of the distribution that dictates the treatment time at which the microorganism or enzyme will fail to resist and result in inactivation.

$$F(t) = \exp\left[-\left(\frac{t}{p}\right)^q\right] \tag{7}$$

This function, first introduced by Peleg and Cole [83] to model microbial survival curves, has been used to describe numerous inactivation kinetics because it is simple (only 2 parameters), flexible, and theoretically sound [1, 7, 11, 13, 23, 59, 86, 89]. For inactivation kinetics studies, Eq. 7 is frequently transformed to a $\log_{10}$ base of the survival fraction $S(t)$ as in Eq. 8 [86] or Eq. 9 [22]:

$$\log_{10}\frac{N}{N_0} = \log_{10} S(t) = -\frac{1}{2.303}\cdot\left(\frac{t}{b}\right)^n \tag{8}$$

$$\log_0 S(t) = -b'\cdot t^n \tag{9}$$

The parameter n determines the shape of the survival curve (Fig. 1a), where $n < 1$ denotes upward concavity and $n > 1$ represents a downward concavity while $n = 1$ would be a *unique* case corresponding to linear or first-order kinetics. Concavity can be used to interpret the population inactivation resistance: (a) homogenous ($n = 1$), (b) tailing or increasing resistance ($n < 1$), or (c) decreasing resistance as a result of accumulated damage to the population ($n > 1$) [86]. Although these three resistance behaviors have been observed in modeling work, no microbial physiology studies have been conducted to confirm them

Table 1 Reported values for the first-order inactivation-related kinetics and related models

Target	Medium	Pressure Come up time Holding time Depressurization Temperature	Kinetic model	Model parameters	Regression software	Reference
Aerobic bacteria	Fresh, whole, raw milk pH 6.64 7.68 × 10^7 cfu ml^{-1} inoculum	300, 400, 600 MPa 100–200 MPa s^{-1} 0–105 min NR 25 °C	First order (Eq. 3) *D* value (Eq. 4)	k = 0.1643–0.7576 min^{-1} D_P = 3.04–14.03 min	SigmaPlot 8.0	Dogan and Erkmen [29]
Aerobic bacteria	Fresh, filtered orange juice pH 3.35 5.71 × 10^7 cfu ml^{-1} inoculum	300, 400, 600 MPa 100–200 MPa s^{-1} 0–30 min NR 25 °C	First order (Eq. 3) *D* value (Eq. 4)	k = 0.5152–1.8573 min^{-1} D_P = 1.24–4.47 min	SigmaPlot 8.0	Dogan and Erkmen [29]
Aerobic bacteria	Fresh, filtered peach juice pH 5.21 5.75 × 10^7 cfu ml^{-1} inoculum	300, 400, 600 MPa 100–200 MPa s^{-1} 0–70 min NR 25 °C	First order (Eq. 3) *D* value (Eq. 4)	k = 0.2357–1.0812 min^{-1} D_P = 2.13–9.77 min	SigmaPlot 8.0	Dogan and Erkmen [29]
Aerobic bacterial spores	Deionized water *B. amyloliquefaciens* TMW 2.479 Fad 82 *B. amyloliquefaciens* TMW 2.482 Fad 11/2 *B. sphaericus* NZ 14 *B. amyloliquefaciens* ATCC 49763	700 MPa 0.58 min 0–5 min NR 105, 121 °C	*D* value (Eq. 4)	D_P = 0.30–0.60 min (105 °C) D_P = 0.10–0.50 min (121 °C)	Microcal Origin 7.5	Ahn et al. [1]
Anaerobic bacterial spores	Deionized water *C. sporogenes* ATCC 7955 *C. tyrobutylicum* ATCC 27384 *T. thermosaccharolyticum* ATCC 27384	700 MPa 0.58 min 0–5 min NR 105, 121 °C	*D* value (Eq. 4)	D_P = 0.20–0.60 min (105 °C) D_P = 0.30 min (121 °C)	Microcal Origin 7.5	Ahn et al. [1]
Bacillus stearothermophilus spores	Egg Defrosted egg patties 10^6 spores g^{-1} inoculum	400, 600, 700 MPa 1.9–2.4 min 0–16 min NR 105.8 ± 0.6 °C	*D* value (Eq. 4)	D_P = 0.41–0.72 min	SAS	Rajan et al. [91]

Table 1 continued

Target	Medium	Pressure Come up time Holding time Depressurization Temperature	Kinetic model	Model parameters	Regression software	Reference
Escherichia coli	Fresh extracted carrot juice pH 6.6 K-12 strain MG1655 10^9 cfu ml^{-1} inoculum	200, 250, 300, 350, 400, 450, 500, 550, 600 MPa 100 MPa min^{-1} 0–60 min NR 5–45 °C	*D* value (Eq. 4)	D_P = 2.00–188.00 min	SAS online DOC 8.01	Van Opstal et al. [114]
Listeria monocytogenes	Fresh, whole, raw milk pH 6.64 7.48 x 10^7 cfu ml^{-1} inoculum	300, 400, 600 MPa 100–200 MPa s^{-1} 0–105 min NR 25 °C	First order (Eq. 3) *D* value (Eq. 4)	k = 0.2096–0.9477 min^{-1} D_P = 2.43–10.99 min	SigmaPlot 8.0	Dogan and Erkmen [29]
Listeria monocytogenes	Fresh, filtered orange juice pH 3.35 2.93 × 10^7 cfu ml^{-1} inoculum	300, 400, 600 MPa 100–200 MPa s^{-1} 0–30 min NR 25 °C	First order (Eq. 3) *D* value (Eq. 4)	k = 0.8024–2.6471 min^{-1} D_P = 0.87–2.87 min	SigmaPlot 8.0	Dogan and Erkmen [29]
Listeria monocytogenes	Fresh, filtered peach juice pH 5.21 2.95 × 10^7 cfu ml^{-1} inoculum	300, 400, 600 MPa 100–200 MPa s^{-1} 0–70 min NR 25 °C	First order (Eq. 3) *D* value (Eq. 4)	k = 0.3733–1.5151 min^{-1} D_P = 1.52–6.17 min	SigmaPlot 8.0	Dogan and Erkmen [29]
Native microflora	Unpasteurized Hamlin variety orange juice pH 3.7, 10.7°Brix	350, 400, 450, 500 MPa 45–60 s 1–300 s NR 25 ± 5 °C	First order (Eq. 3) *D* value (Eq. 4)	k = 0.0002–0.0064 min^{-1} D_P = 0.05–1.32 min	NR	Parish [79]
Saccharomyces cerevisae ascospores	Commercial pasteurized orange juice 10^5 cfu ml^{-1} inoculum	350, 400, 450, 500 MPa 45–60 s 1–300 s NR 25 ± 5 °C	First order (Eq. 3) *D* value (Eq. 4)	k = 0.0002–0.041 min^{-1} D_P = 0.07–1.27 min	NR	Parish [79]

Table 1 continued

Target	Medium	Pressure Come up time Holding time Depressurization Temperature	Kinetic model	Model parameters	Regression software	Reference
Saccharomyces cerevisae vegetative cells	Commercial pasteurized orange juice 10^5 cfu ml^{-1} inoculum Several strains	350, 400, 450, 500 MPa 45–60 s 1–300 s NR 25 ± 5 °C	First order (Eq. 3) *D* value (Eq. 4)	$k = 0.0005–0.0137$ min^{-1} $D_P = 0.02–0.63$ min	NR	Parish [79]
Vibrio cholerae	Phosphate-buffered saline 10^8 cfu ml^{-1} inoculum Several strains	200–250 MPa 55–80 s 0–240 s <2 s 8–10 °C (initial)	*D* value (Eq. 4)	$D_P = 2.10–3.38$ min (200 MPa) $D_P = 0.60–0.82$ min (250 MPa)	Microsoft Excel	Cook [20]
Vibrio parahaemolyticus	Phosphate-buffered saline 10^8 cfu ml^{-1} inoculum Several strains	200–250 MPa 55–80 s 0–240 s <2 s 8–10 °C (initial)	*D* value (Eq. 4)	$D_P = 0.88–2.78$ min (200 MPa) $D_P = 0.26–0.60$ min (250 MPa)	Microsoft Excel	Cook [20]
Vibrio vulnificus	Phosphate-buffered saline 10^8 cfu ml^{-1} inoculum Several strains	200–250 MPa 55–80 s 0–240 s <2 s 8–10 °C (initial)	*D* value (Eq. 4)	$D_P = 0.28–0.62$ min (200 MPa)	Microsoft Excel	Cook [20]

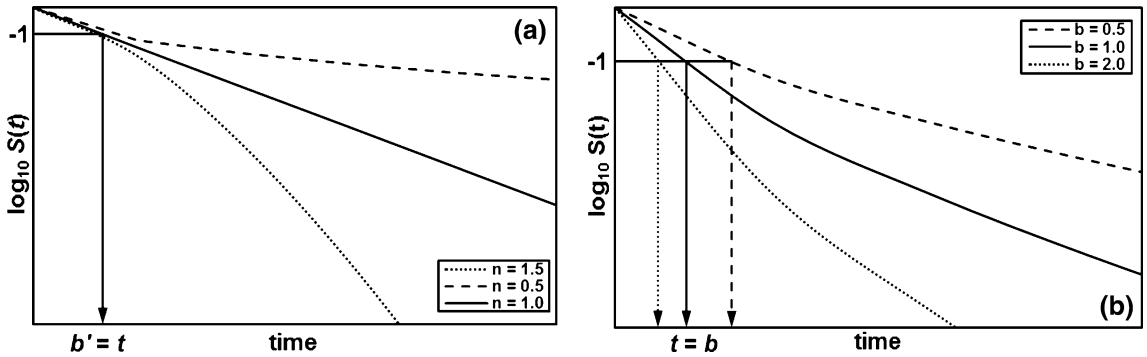

Fig. 1 Influence of the Weibull model parameters on the shape of the microbial survival curve: **a** shape parameter n; **b** scale parameter, b'

experimentally. The parameter b determines the scale of the curve as observed in Fig. 1b [110], whereas the inverse of the rate coefficient b ($b' = 1/2.303\ b^n$) determines the slope steepness of the survival trend [22]. Thus, Eq. 8 can be simplified and expressed as a function of b' (Eq. 9).

As shown in Eqs. 10–12, the inverse of the parameter b' to the -nth power is equivalent to the decimal reduction time (D) determined with the first-order kinetics model [11]:

$$\log_{10}\frac{0.1N_0}{N_0} = -1 = -b' \cdot t^n \tag{10}$$

$$1 = b' \cdot t^n \tag{11}$$

$$t = \left(\frac{1}{b'}\right)^{-n} = D \tag{12}$$

Most studies report HPP survival curves with upward concavities yielding $n < 1$ and $b' < 1$ values for the Weibull model parameters with the latter increasing to values in the 1–3 range and a concurrent decrease in the n parameter for more severe pressure and/or temperature conditions (Table 2). This shows that the accumulated damage theory was fulfilled for most of the values reported in Table 2, since more severe HPP conditions sensitized the population and lowered the shape n parameter ($n < 1$), and higher inactivation rates were observed as the slope increased ($b' > 1$). Although this model has been often applied to predict microbial inactivation kinetics, no reports of its application to model the inactivation of enzymes, also known to display nonlinear trends, were found. Finally, details on the pressure and temperature effects on the Weibull model parameter are discussed in the secondary model section.

Peleg [86] highlighted that nonlinear regression procedures for either ln $S(t)$ or $\log_{10}S(t)$ as a function of t can only estimate the real parameters of the Weibull distribution since deviations occur with the logarithmic transformation of Eq. 7. Furthermore, Mafart et al. [67] claimed that b' and n are strongly correlated, consequently a poor estimation of either one will affect the other parameter.

Sigmoidal Primary Models

Weibull Biphasic Model

Guan et al. [38] found that the single term Weibull model (Eq. 9) was not adequate to describe complex survival curves with more than one concavity change. Coroller et al. [21] encountered this limitation when analyzing the acidic inactivation of *L. monocytogenes* and *Salmonella enterica*. They assumed that two bacterial subpopulations were present, and thus, the Weibull model was reparametrized as a function of the labile population fraction (f) as follows:

$$N(t) = N_0\left[f \cdot 10^{-\left(\frac{t}{b'_1}\right)^{n_1}} + (1-f)\cdot 10^{-\left(\frac{t}{b'_2}\right)^{n_2}}\right] \tag{13}$$

Since microbial data are frequently expressed using a decimal exponential base, the fraction (f) alone may not be useful. Coroller et al. [21] transformed f to a decimal logarithmic base and introduced the parameter ψ in the Weibull multipopulation model (Eqs. 14–15). An example of a survival curve for populations with different subpopulation resistance predicted with the Weibull biphasic model is shown in Fig. 2.

$$\psi = \log_{10}\left(\frac{f}{1-f}\right) \tag{14}$$

$$N(t) = \frac{N_0}{1+10^{\psi}}\left[10^{\left[\psi-\left(\frac{t}{b'_1}\right)^{n_1}\right]} + 10^{-\left(\frac{t}{b'_2}\right)^{n_2}}\right] \tag{15}$$

Coroller et al. [21] simplified Eq. 15 by defining $n = n_1 = n_2$ after demonstrating statistically that the shape parameters of subpopulation 1 (n_1) and subpopulation 2 (n_2) did not differ significantly ($p_{\text{value}} < 0.05$). The model resulting from this simplification (Eq. 16) yielded a slightly more accurate fit while reducing the number of parameters for the nonlinear regression.

Table 2 Reported parameters for the primary Weibull model describing HPP inactivation kinetics

Target	Medium	Pressure Come up time Holding time Depressurization Temperature	Model parameters	Regression software	Reference
Aerobic bacterial spores	Deionized water *B. amyloliquefaciens* TMW 2.479 Fad 82 *B. amyloliquefaciens* TMW 2.482 Fad 11/2 *B. sphaericus* NZ 14 *B. amyloliquefaciens* ATCC 49763	700 MPa 0.58 min 0–5 min NR 105, 121 °C	$b' = 1.5–3.1$ (105 °C); 2.1–6.5 (121 °C) $n = 0.2–0.5$ (105 °C); 0.3–1.0 (121 °C)	Microcal Origin 7.5	Ahn et al. [1]
Anaerobic bacterial spores	Deionized water *C. sporogenes* ATCC 7955 *C. tyrobutylicum* ATCC 27384 *T. thermosaccharolyticum* ATCC 27384	700 MPa 0.58 min 0–5 min NR 105, 121 °C	$b' = 1.5–3.2$ (105 °C); 1.7–2.8 (121 °C) $n = 0.2–0.5$ (105 °C); 0.5–0.7 (121 °C)	Microcal Origin 7.5	Ahn et al. [1]
Bacillus coagulans spores	Phosphate buffer (100 mM, pH 6.7) 10^6 cfu ml^{-1} inoculum IFFI 10144 strain	400–600 MPa 3.1–4.6 min 0–30 min NR 70–80 °C (initial temperature)	$b' = 1.977–2.622$ (70 °C); 1.553–3.447 (80 °C) $n = 0.160–0.207$ (70 °C); 0.124–0.260 (80 °C)	SPSS 13.0	Wang et al. [119]
Bacillus stearothermophilus spores	Egg Defrost egg patties 10^6 spores g^{-1} inoculum	400, 600, 700 MPa 1.9–2.4 min 0–16 min NR 105.8 ± 0.6 °C	$b' = 1.30–1.96$ $n = 0.30–0.54$	SAS	Rajan et al. [91]
Escherichia coli	Whey protein surrogate food system ATCC 11229 strain	207–439 MPa NR 0–300 min NR 30, 40, 50 °C	$b' = 2.7 \times 10^{-8}$–0.482 (30 °C); 4.0x10^{-4}–2.161 (40 °C); 3.0×10^{-3}–2.653 (50 °C) $n = 0.70–3.37$ (30 °C); 0.36–2.24 (40 °C); 0.48–1.81 (50 °C)	NR	Doona et al. [31]
Escherichia coli	UHT whole milk pH 6.64 10^8 cfu ml^{-1} inoculum ATCC 11775 strain	400, 450, 500, 550, 600 MPa 300 MPa min^{-1} 0–80 min 300 MPa min^{-1} 22 °C	$b' = 1.2–10.5$ $n = 0.78$	SigmaPlot 2000 6.0	Buzrul et al. [11]
Listeria innocua	UHT whole milk pH 6.64 10^8 cfu ml^{-1} inoculum ATCC 33090 strain	400, 450, 500, 550, 600 MPa 300 MPa min^{-1} 0–80 min 300 MPa min^{-1} 22 °C	$b' = 1.1–12.2$ $n = 0.79$	SigmaPlot 2000 6.0	Buzrul et al. [11]

Table 2 continued

Target	Medium	Pressure Come up time Holding time Depressurization Temperature	Model parameters	Regression software	Reference
Listeria innocua	Peptone solution 0.1 % CDW47 strain 10^8–10^9 cfu ml^{-1} inoculum	138, 207, 276, 345 MPa 300 MPa min^{-1} 0–30 min <1 min 25, 35, 45, 50 °C	b' = 0.09–0.21 (25 °C); 0.01–0.03 (35 °C); 0.002–2.12 (45 °C); 0.19–4.38 (50 °C) n = 0.45–0.79 (25 °C); 0.64–1.26 (35 °C); 0.35–1.87 (45 °C); 0.23–1.14 (50 °C)	SigmaPlot 2000 6.0	(Buzrul and Alpas [10]
Yersinia enterocolitica	UHT whole milk pH 6.70 5×10^8 cfu ml^{-1} inoculum ATCC 35669 strain	400–500 MPa	b' = 0.66 (400 MPa); 1.13 (500 MPa) Calculated from linear approach[a] n = 0.583	SAS 8.2	Chen and Hoover [15]

[a] The corresponding values of parameter b' in the Weibull equation come from the empirical equation $b' = 0.0047 * P - 1.2191$ obtained by Chen and Hoover [15]

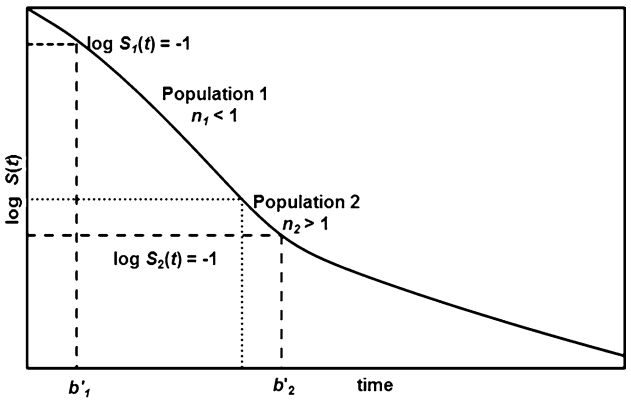

Fig. 2 Influence of Weibull biphasic model parameters on the shape of the microbial survival curve

$$N(t) = \frac{N_0}{1 + 10^{\psi}} \left[10^{\left[\psi - \left(\frac{t}{b'_1} \right)^n \right]} + 10^{-\left(\frac{t}{b'_2} \right)^n} \right] \tag{16}$$

Log-Logistic Model

Cole et al. [19] developed a model to predict bacterial inactivation following sigmoidal survival curves starting from the four parameter model shown in Eq. 17.

$$y = \alpha + \frac{\beta}{1 + \exp(\lambda - \delta \cdot x)} \tag{17}$$

The authors attempted to confer a biological interpretation to the parameters of Eq. 17 by applying the first and second derivative criterions (Eqs. 18–19) to obtain the maximum inactivation rate (Ω), and the time at which Ω occurs (τ). Afterward, Cole et al. [19] defined the dependent variable as the microbial population logarithm ($y = \log_{10} N$) and the independent variable as the logarithm of time ($x = \log_{10} t$). Parameter ω was defined as the difference between the lower and upper asymptotes ($\omega = \beta - \alpha$), and all three biological parameters (Ω, τ, ω) were incorporated into Eq. 17 to obtain Eq. 20. Although the expression $\log_{10}(N_{t=0})$ cannot be calculated since $\log_{10}(t = 0)$ is mathematically undefined, the expression $\log_{10}(N/N_0)$ is more commonly used to describe microbial inactivation kinetics than $\log_{10}(N)$. The authors gave no justification but assumed that $t = 0.1$ min was a good approximation for $t = 0$ min to establish the "vitalistic" log-logistic model (Eq. 21).

$$y'' = \frac{d^2 y}{dx^2} = 0 = \lambda - \delta \cdot x; \quad x = \tau = \frac{\lambda}{\delta} \tag{18}$$

$$y'\left(x = \frac{\lambda}{\delta} \right) = \frac{dy}{dx} = \frac{\delta \cdot \beta}{4}; \quad \Omega = \frac{\delta \cdot \beta}{4} \tag{19}$$

$$\log_{10} N = \alpha + \frac{\omega - \alpha}{1 + \exp\left[\frac{4\cdot\Omega}{\omega-\alpha}(\tau - \log_{10} t)\right]} \tag{20}$$

$$\log_{10} N = \frac{\omega - \alpha}{1 + \exp\left[\frac{4\cdot\Omega}{\omega-\alpha}(\tau - \log_{10} t)\right]} - \frac{\omega - \alpha}{1 + \exp\left[\frac{4\cdot\Omega}{\omega-\alpha}(\tau + 1)\right]} \tag{21}$$

Moreover, the application of the logarithm function to the independent variable ($x = \ln t$) should have been performed prior to the derivation of Eq. 17. The evaluation of the second derivative of Eq. 17 shown in Eq. 22 indicates that the solution presented by the authors as Eq. 18 is only valid when the parameter $\delta \to \infty$. The estimation of parameters τ and Ω depends on δ being sufficiently large ($\delta \to \infty$) as seen in Eqs. 18, 22. Unfortunately, we could not find if Cole et al. [19] reported whether this condition ($\delta \to \infty$) is attained for either thermal or high-pressure processing microbial inactivation. Users of this model should evaluate whether the parameter delta is sufficiently large ($\delta \to \infty$) to validate the biological interpretability of the log-logistic model parameters.

$$y'' = \frac{\mathrm{d}^2 y}{\mathrm{d}(\ln x)^2} = \lambda + \ln\left(\frac{\delta - 1}{\delta + 1}\right) = \delta \cdot \ln x \tag{22}$$

Chen and Hoover [15] were among the first investigators to use a slightly modified "vitalistic" log-logistic model to analyze microbial inactivation by HPP (Eq. 23). These authors defined the parameter H as the difference between the upper and lower asymptotes ($H = \alpha - \beta$) and $t \sim 0$ as $t = 10^{-6}$ min. As in the case of Cole et al. [19], Chen and Hoover [16] gave no explanation for the use of this latter value. The model was evaluated for the inactivation of *Yersinia enterocolitica* in sodium potassium buffer and in UHT whole milk subjected at room temperature to pressures within the 300–500 MPa range. The experimental survival data were described using the linear, Weibull, Gompertz, and log-logistic models to identify the best inactivation model. Amidst the models tested, the log-logistic equation was most consistently the best model as denoted by its regression coefficient ($R^2 = 0.946$–0.982) and accuracy factor ($A_f = 1.047$–1.144). The values reported in Table 3 for the H parameter ranged from -4.61 to -39.71, which clearly lacks a biological or physical meaning. Consequently, Chen and Hoover [15] decided to fix $H = -14$, which reduced also the number of parameters (Eq. 24). Although a clear reason for selecting this value was not provided, the reduced log-logistic model (Eq. 24) gave slightly better results than the three-parameter model (Eq. 23) as shown in Fig. 3.

$$\log\frac{N}{N_0} = \frac{H}{1 + \exp\left[\frac{4\cdot\Omega\cdot(\tau - \log t)}{H}\right]} - \frac{H}{1 + \exp\left[\frac{4\cdot\Omega\cdot(\tau+6)}{H}\right]} \tag{23}$$

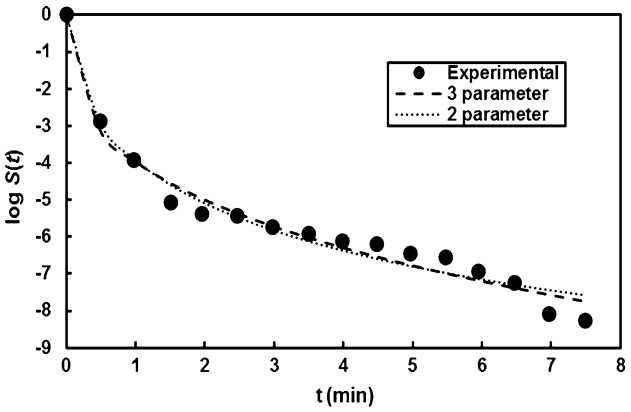

Fig. 3 Log-logistic inactivation curve modeling for *Yersinia enterocolitica* survival in sodium phosphate buffer (0.1 M, pH 7) at 450 MPa and room temperature, modified from Chen and Hoover [15, 16]

$$\log\frac{N}{N_0} = -\frac{14}{1 + \exp\left[-\frac{\sigma\cdot(\tau - \log t)}{3.5}\right]} + \frac{14}{1 + \exp\left[-\frac{\sigma\cdot(\tau+6)}{3.5}\right]} \tag{24}$$

Additional Weibull and log-logistic HPP inactivation kinetic model comparisons have been published for diverse pathogens and food matrixes [10, 17, 38, 39, 53, 119] showing equally acceptable or slightly better predictions when using Eq. 23. The greatest advantage of the log-logistic over the Weibull model is its ability to describe sigmoidal kinetic curves without further modifications [38]. However, only a few values of the log-logistic model parameters have been reported for HPP (Table 3), and no secondary models to predict pressure and temperature effects on the parameters H, Ω, or τ were found when preparing this review.

Other Primary Models

Other primary models commonly found for the temperature effect on microbial growth and microbial/enzyme inactivation kinetics have been used to a lesser extent when analyzing combined pressure and temperature effects on foods. They include the Baranyi–Roberts equation [4, 88, 100], the Gompertz model, which has consistently shown poorer fit when compared to other primary models [15, 38, 56, 100, 116], and the enhanced quasi-chemical kinetic model (EQCKM). Even though the latter accounts for only a few publications in the high-pressure kinetics area, this model was further analyzed in this review as it represented a recent and very different modeling approach.

Enhanced Quasi-Chemical Kinetic Model (EQCKM)

Unlike most microbial predictive models that take into account only the population growth or inactivation rate

Table 3 Reported parameters for the primary log-logistic model describing HPP inactivation kinetics

Target	Medium	Pressure Come up time Holding time Depressurization Temperature	Kinetic model	Model parameters	Regression software	Reference
Bacillus coagulans spores	Phosphate buffer 100 mM, pH 6.7 10^6 cfu ml^{-1} inoculum IFFI 10144 strain	400–600 MPa 3.1–4.6 min 0–30 min NR 70–80 °C (initial temperature)	3 parameter (Eq. 23)	$H = -(4.611–18.848)$ 70 °C $H = -(4.754–5.938)$ 80 °C $\Omega = -(1.871–2.074)$ 70 °C $\Omega = -(1.726–2.953)$ 80 °C $\tau = 0.449–3.956$ (70 °C) $\tau = 0.011–1.049$ (80 °C)	SPSS 13.0	Wang et al. [119]
Listeria innocua	Peptone solution 0.1 % CDW47 strain 10^8–10^9 cfu ml^{-1} inoculum	138, 207, 276, 345 MPa 300 MPa min^{-1} 0–30 min <1 min 25, 35, 45, 50 °C	3 parameter (Eq. 23)	$H = -(4.92–23.39)$ 25 °C $H = -(2.89–15.08)$ 35 °C $H = -(1.26–56.24)$ 45 °C $H = -(1.37–39.71)$ 50 °C Ω = NR τ = NR	SigmaPlot 2000 6.0	Buzrul and Alpas [10]
Yersinia enterocolitica	UHT whole milk pH 6.70 5×10^8 cfu ml^{-1} inoculum ATCC 35669 strain	350–500 MPa	3 parameter (Eq. 23)	$H = -(9.878–27.884)$ $\Omega = -(7.748–11.199)$ $\tau = 1.478–2.100$	SAS 8.2	Chen and Hoover [15]
Yersinia enterocolitica	UHT whole milk pH 6.70 5×10^8 cfu ml^{-1} inoculum ATCC 35669 strain	350–500 MPa	2 parameter (Eq. 24)	$H = -14$ $\Omega = -(6.944–10.324)$ $\tau = 1.380–1.989$	SAS 8.2	Chen and Hoover [15]

kinetics, the quasi-chemical model can describe both phenomena individually or simultaneously [98]. According to the quasi-chemical kinetic model (QCKM), biochemical reactions occurring at the microbial level can be assumed to follow a successive four-step chemical kinetics mechanism representing (1) transition of microbial cells from the lag phase to the growth stage, (2) multiplication of microorganisms in the growth phase on a binary exponential basis, (3) microbial death after completing the cell life cycle, and (4) microbial death by the accumulation of a nonspecific hazardous metabolite.

A set of chemical reaction equations relating rate constants (k) with the microbial population or the hazardous metabolite concentration can be developed for each step and solved as a system of ordinary differential equations [31, 98]. The QCKM was originally developed for the predictions of pathogen growth under various environmental conditions differing in pH, a_w, and concentration of an added microbial inhibitor [98]. The same approach has been successfully applied to model the kinetics for the pressure inactivation of *Escherichia coli* in the 207–345 MPa and 30–50 °C range [30]. The quasi-chemical model effectively fit sigmoidal curves for *E. coli* at 40–50 °C and shoulder formation but only under the mildest experimental conditions [30, 31]. Furthermore, Doona et al. [32] reported that the QCKM failed to describe well the high-pressure kinetics for the inactivation of *L. monocytogenes*, which presented "tailing." Therefore, the authors adapted the differential equations of the QCKM under a new set of theoretical assumptions for the complete cell cycle under high pressure and renamed it as the "enhanced" quasi-chemical kinetic model (EQCKM).

A modified version of the EQCKM considering only microbial inactivation under high pressure is shown in Fig. 4. Under the assumptions of this EQCKM version, the population of microbial cells in the lag phase (M) subjected to pressure can either become metabolically active to propagate a population in the growth phase (M*) at a very slow rate (Eq. 25), or remain in the lag phase while displaying superior baroresistance (BR; Eq. 26). Finally, both M* and BR undergo inactivation at different rates (MD, Eqs. 27–28). First-order kinetics was assumed to describe the change with time of all microbial populations assumed in this modified model (M, M*, BR, D). Thus, each step of the EQCM (Fig. 4) corresponds to a biochemical reaction with a kinetic rate constant (k_1–k_4). Due to the presence of successive biochemical reactions, all differential equations must be solved simultaneously as shown in the analytical solution (Eq. 29aa–c). However, the "true" microbial count values for M, M*, and BR cannot be determined experimentally. The experimental quantification of *L. monocytogenes* after each HPP treatment can describe only the total of the individual populations assumed in the model ($U = M + M^* + \mathrm{BR}$; Eq. 29dd) and not their individual values. The EQKM solution is found by minimizing the error between the experimental microbial plate counts (U) and sum of the predicted values.

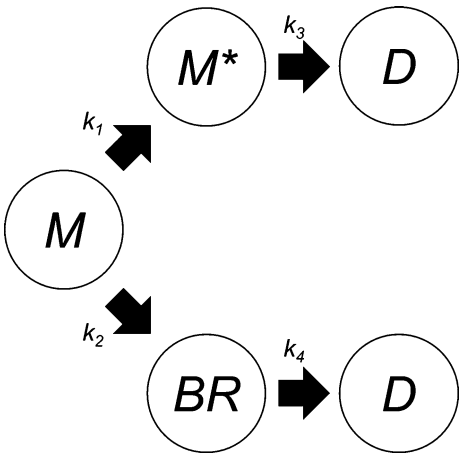

Fig. 4 Modified version of the enhanced quasi-chemical kinetic model (EQCKM) scheme describing microbial inactivation under high pressure; M microbial cells in lag phase, M* metabolically active microbial cells in the growth phase, BR baroresistant microbial population, D dead microbial cells, modified from Doona et al. [32]

$$M \rightarrow M^*, k_1 \tag{25}$$

$$M \rightarrow \mathrm{BR}, k_2 \tag{26}$$

$$M^* \rightarrow \mathrm{MD}, k_3 \tag{27}$$

$$\mathrm{BR} \rightarrow \mathrm{MD}, k_4 \tag{28}$$

$$\frac{\mathrm{d}M}{\mathrm{d}t} = -(k_1 + k_2) \cdot M \tag{29a}$$

$$\frac{\mathrm{d}M^*}{\mathrm{d}t} = k_1 \cdot M - k_3 \cdot M* \tag{29b}$$

$$\frac{\mathrm{dBR}}{\mathrm{d}t} = k_2 \cdot M - k_4 \cdot \mathrm{BR} \tag{29c}$$

$$U = M + M^* + \mathrm{BR} \tag{29d}$$

Since the EQCKM describes two different inactivation rates, Doona et al. [32] opted to validate the model by calculating the processing time (t_p) required to deliver 6-log reductions in *L. monocytogenes* counts (U) for several pressure (207–414 MPa) and temperature (20–50 °C) combinations. The model successfully predicted t_p as shown by the low standard error values (0.09–0.46) in the pressure–temperature range studied. For all pressure/temperature combinations, the kinetic constants k_1 and k_3 were greater than k_2 and k_4. The differences became more evident at 414 MPa, indicating that the microbial inactivation is primarily driven by pressure in the 20–50 °C temperature range. Additionally, the high-pressure resistance of *L. monocytogenes* was confirmed since k_3 was only significantly higher than k_4 for pressure levels over 345 MPa, and

Table 4 Reported parameters for an attempted global Bigelow secondary model. Modified from Santillana Farakos and Zwietering [99]

Microorganism	D samples	P range (MPa)	T range (°C)	R^2_{adj}	z_P	z_T	log $D_{PrefTref}$	P_{ref} (MPa)	T_{ref} (°C)
Bacillus spp. spores	48	100–700	45–121	0.86	614.7 ± 122.9	45.2 ± 6.5	0.27 ± 0.25	400	100
Clostridium spp. spores	54	600–900	80–121	0.88	616.3 ± 106.3	20.4 ± 1.1	0.85 ± 0.36	400	100
Cronobacter spp.	24	200–600	22–25	0.78	368.2 ± 39.4	NR	−0.19 ± 0.13	400	NR
Escherichia coli	117	100–700	2–50	0.30	385.6 ± 53.2	97.5 ± 45.2	0.88 ± 0.23	400	30
Listeria spp.	74	200–700	2–50	0.61	298.9 ± 34.6	38.6 ± 7.5	0.56 ± 0.18	400	30
Vibrio spp.	80	69–345	10–25	0.61	206.9 ± 32.0	−18.4 ± 2.3	0.06 ± 0.20	400	30
Zygosaccharomyces bailii	48	100–400	−5 to 45	0.71	91.0 ± 8.4	141–7 ± 58.6	−0.84 ± 0.24	400	30

just three of the tested PATP treatments yielded $t_p \leq 15$ min. A key disadvantage of the EQCKM is that the key variables involved (M, M^*, and BR) and their relationship to experimental microbial plate counts (U; Eq. 29dd) remain a theoretical construct that will be difficult to confirm experimentally.

Secondary Models

The previously reviewed primary models are useful when the processing conditions (pressure, temperature, pH, etc.) are kept constant. If any processing condition is changed, a new set of experiments must be performed to obtain new primary model parameters. To extend the application of primary models, mathematical expressions known as secondary models can be developed to estimate the pressure and/or temperature effect on the predicted primary model parameters. As in the case of primary models, secondary models can be obtained from theoretical considerations or empirical observations. Most of the secondary models here presented are nonlinear, reflecting complex biological behaviors under high-pressure/high-temperature conditions.

Simultaneous Pressure and Temperature Effects on First-Order Kinetics Parameters

Bigelow Model

The Bigelow model was developed to obtain log-linear estimates of the decimal reduction time as a function of temperature [8, 71, 72]. The equation became so important and broadly accepted that even nowadays, it remains the standard approach in thermal processing design [25, 46, 109].

The Bigelow model has been adopted to model the reaction rate dependence on the applied pressure ($k(P)$) using z_P, defined as the inverse negative slope of log D_P versus pressure level (Eq. 30). The parameter z_P determines the pressure increase required to achieve a tenfold increase in the inactivation rate, a constant analogous to the thermal resistance constant z_T [20, 29, 55, 57, 79, 86, 94, 114, 126].

$$z_p = -\frac{P - P_{ref}}{\log D_p - \log D_{P_{ref}}} \tag{30}$$

Santillana Farakos and Zwietering [99] attempted to establish a global kinetic model based on the pressure and temperature dependence of the microbial inactivation kinetics by HPP. Reported D values for first-order kinetics (Table 4) were fitted to Eqs. 30–32 and analyzed statistically. Both models for D (Eqs. 31–32) assume that the exponential relation of z_P and z_T was directly proportional to pressure and temperature; however, Eq. 32 includes a term describing a first-order interaction between pressure and temperature. The parameter z_{PT} represents the amount that the linear term $P \cdot T$ needs to increase for a tenfold decrease in D.

$$\log D = \frac{1}{z_P} \cdot (P_{ref} - P) + \frac{1}{z_T} \cdot (T_{ref} - T) + \log D_{PrefTref} \tag{31}$$

$$\log D = \frac{1}{z_P} \cdot \left(P_{ref} - P\right) + \frac{1}{z_T} \cdot \left(T_{ref} - T\right) + \frac{1}{z_{PT}} \cdot \left[\left(T_{ref} \cdot P_{ref}\right) - (T \cdot P)\right] + \log D_{Pr\,efTref} \tag{32}$$

Santillana Farakos and Zwietering [99] showed for Eq. 30 the lowest adjusted regression coefficient ($R^2_{adj} = -0.037$ to 0.630) reflecting the large influence of temperature on HPP treatments. Both models describing the pressure–temperature effect (Eqs. 31–32) had similar prediction accuracy ($R^2_{adj} = 0.30$–0.87), indicating that the linear pressure–temperature interaction has no overall significance ($p_{value} > 0.05$). Thus, Santillana Farakos and Zwietering [99] reported only the parameters for Eq. 31 (Table 4). Bacterial spores displayed the highest pressure resistance constant ($z_P = 614$–616 MPa), followed by vegetative cells ($z_P = 206$–385 MPa) and yeasts ($z_P = 91$ MPa). Conversely, under high pressure, the temperature effect on yeast inactivation was less significant ($z_T = 141$ °C) than the

observed for vegetative cells (z_T = 38–97 °C) and spores (z_T = 20–45 °C), since yeasts are readily inactivated by pressure alone. The *Vibrio* species (spp.) was the only microorganism to be more readily inactivated when temperature was lowered ($z_T = -18.4 \pm 2.3$). The authors highlighted the need to avoid using these models for non-linear inactivation curves, since under- or overestimation may occur (Santillana Farakos and Zwietering [99].

Pressure Kinetics Fundamentals

The Le Chatelier principle states that *under equilibrium*, a system subjected to pressure will adopt the molecular configurations, chemical interactions, and chemical reactions yielding the smallest overall volume [3, 35, 123]. Mathematically, the Le Chatelier principle has been expressed with thermodynamic relations by using the partial molar volume (V) concept originally defined for gas mixtures. The overall molar volume change for the reaction ($\Delta\overline{V}_{\text{reaction}}$) defined as the difference in the partial molar volumes of products and reactants (Eq. 33) can be expressed as the change of the Gibbs energy with respect to pressure at a constant temperature. Thus, $\Delta\overline{V}_{\text{reaction}}$ is related directly to the equilibrium constant (K) for the reaction [104].

$$\Delta\overline{V}_{\text{reaction}} = \sum \overline{V}_{\text{P}} - \sum \overline{V}_{\text{R}} = \left(\frac{\partial \Delta G}{\partial P}\right)_T = -RT\left(\frac{\partial \ln K}{\partial P}\right)_T \tag{33}$$

This description is further extrapolated to biological systems under the *Transitional State Theory* by proposing the existence of a biological reactant (R) in equilibrium with an activated biological complex ($X^{\neq}$) prior to the formation of the biological reaction product P (Eq. 34). If the formation of the activated complex is in thermal equilibrium, the frequency ($\upsilon^{\neq}$) at which $X^{\neq}$ transforms into P can be calculated using quantum ($E = h \cdot \upsilon^{\neq}$) and classical physics ($E = k_B \cdot T/h$)) equations describing the internal energy distribution (Eq. 35):

$$R \overset{K^{\neq}}{\leftrightarrow} X^{\neq} \overset{\upsilon^{\neq}}{\longrightarrow} P \tag{34}$$

$$\upsilon^{\neq} = \frac{k_{\text{B}} \cdot T}{h} \tag{35}$$

where h is the Planck constant (6.626×10^{-34} J s^{-1}), k_B is the Boltzmann constant (1.38×10^{-23} J K^{-1}), and T (K) is the absolute temperature at which the chemical reaction takes place [58, 70]. Hence, the product formation rate equation (r_P; Eq. 36) can be rewritten to yield Eq. 38 by substituting $\upsilon^{\neq}$ (Eq. 35) and the pseudo-equilibrium constant $K^{\neq}$ (Eq. 37) to obtain a theoretical definition of the kinetic rate constant k (Eq. 39).

$$r_{\text{P}} = \upsilon^{\neq} \cdot \left[X^{\neq}\right] \tag{36}$$

$$K^{\neq} = \frac{\left[X^{\neq}\right]}{[R]} \tag{37}$$

$$r_{\text{P}} = \frac{k_{\text{B}} \cdot T}{h} \cdot K^{\neq} \cdot [R] \tag{38}$$

$$k = \frac{k_B \cdot T}{h} \cdot K^{\neq} \tag{39}$$

To depict the effect of pressure on the kinetic rate constant for isothermal conditions, Eq. 39 can be used to substitute $K^{\neq}$ in Eq. 33. The Gibbs free energy and volume change are state functions and a reference pressure (P_{ref}) must be selected arbitrarily when quantifying these thermodynamic properties. By integrating Eq. 40 from P_{ref} to P and defining the kinetic constant with respect to the reference conditions (k_{ref}) yields the Eyring model (Eq. 42), where the term $h/k_B \cdot T$ is a constant and its derivative equals zero (Eq. 41).

$$\left[\frac{\partial \ln K^{\neq}}{\partial P}\right]_T = \frac{\partial}{\partial P}\left[\ln\left(\frac{k \cdot h}{k_B \cdot T}\right)\right]_T \tag{40}$$

$$\frac{\partial}{\partial P}\left[\ln k + \ln\left(\frac{h}{k_B \cdot T}\right)\right]_T = \left[\frac{\partial(\ln k)}{\partial P}\right]_T = -\frac{\Delta V^{\neq}}{R \cdot T} \tag{41}$$

$$\ln k = \ln k_{\text{ref}} - \frac{\Delta V^{\neq} \cdot (P - P_{\text{ref}})}{R \cdot T} \tag{42}$$

According to the Eyring equation (Eq. 42), the slope of the plot ln k versus P under isothermal conditions is an estimation of the volume change between the activated complex and the reactants ($\Delta V^{\neq}$) also known as the *activation volume*. Thus, the formation of the active complex and/or products is accelerated when the activation volume is decreased ($\Delta V^{\neq} < 0$) [44]. Conversely, $\Delta V^{\neq} > 0$ suggests that pressure will inhibit the active complex formation and/or its subsequent transformation into products, whereas $\Delta V^{\neq} = 0$ indicates that the reaction rate is not affected by pressure. The pressure dependence of $\Delta V^{\neq}$ commonly deviates from the linear behavior dictated by the Eyring model (Eq. 42) and either theoretical or empirical approximations must be followed, as discussed in the following sections [47, 51, 101, 112, 120].

It is also important to stress that the *Transition State Theory* is an extension of the collision rate theory of gas phase kinetics. Although the *Transition State Theory* is apparently valid to describe both gas and liquid phase kinetics in practice, a rigorous theoretical approach to liquid phase kinetics involves the determination of other critical features such as electrochemical and transport phenomena properties of all components in the solution [2], which would be very challenging and probably impossible to determine in complex matrixes such as foods.

Eyring–Arrhenius Model

A mathematical model describing the combined effects of pressure (P) and temperature (T) on the inactivation rate constant (k) developed from the exponential form of the Eyring (Eq. 43) and Arrhenius equations (Eq. 44) has been reported by several authors [52, 90, 112, 121].

$$k(P) = k_{\text{refP}} \cdot \exp\left[-\frac{\Delta V^{\neq}(T)}{R} \cdot \frac{(P - P_{\text{ref}})}{T}\right] \quad (43)$$

$$k(T) = k_{\text{refT}} \cdot \exp\left[-\frac{E_a(P)}{R} \cdot \left(\frac{1}{T} - \frac{1}{T_{\text{ref}}}\right)\right] \quad (44)$$

The value of the activation energy (E_a) and activation volume ($\Delta V^{\neq}$) parameters change with the vessel pressure and temperature, respectively. For example, the inactivation rate of orange juice pectinmethylesterase (PME, 100–800 MPa, 30–60 °C) showed a linear dependence of $\Delta V^{\neq}$ with respect to temperature (Eq. 45), whereas E_a and pressure were related exponentially (Eq. 46) [90].

$$\Delta V^{\neq}(T) = a \cdot (T - T_{\text{ref}}) + \Delta V_{\text{T}}^{\neq} \quad (45)$$

$$E_a(P) = E_{aP} \cdot \exp[-g \cdot (P - P_{\text{ref}})] \quad (46)$$

The double integration of the inactivation rate constant (k) with respect to pressure and temperature yields Eq. 47:

$$k = k_{\text{refP,T}} \cdot \exp\left\{-\frac{E_{\text{aP}}}{R} \cdot \exp[-g \cdot (P - P_{\text{ref}})] \cdot \left(\frac{1}{T} - \frac{1}{T_{\text{ref}}}\right) - \frac{a \cdot (T - T_{\text{ref}}) + \Delta V_{\text{T}}^{\neq}}{R} \cdot \frac{P - P_{\text{ref}}}{T}\right\} \quad (47)$$

This particular model deviated at low pressure (100–250 MPa) and moderate temperature ranging from 30 to 40 °C [90], and therefore these conditions were not taken into account for $k(P, T)$ predictions (Fig. 5a). However, Katsaros et al. [52] obtained a good correlation ($R^2 = 0.993$) between experimental and predicted values of orange PME inactivation within 100–500 MPa and 20–40 °C when applying the same model (Fig. 5b). The different outcomes obtained by Polydera et al. [90] and Katsaros et al. [52] may reflect differences in the orange variety and experimental conditions used. Although the Eyring–Arrhenius modeling of the experimental data was performed using the same software, differences were observed in the estimated activation energy (Table 5), i.e., $E_a = 148$ kJ mol^{-1} [90] and $E_a = 95$ kJ mol^{-1} [52]. It should be noted that the latter authors used narrower pressure and temperature ranges, and the reference conditions (P_{ref}, T_{ref}) for Eq. 47 were not the same. Katsaros et al. [52] chose 300 MPa and 308 K, whereas Polydera et al. [90] selected reference conditions close to the region with the most significant enzymatic inactivation observed

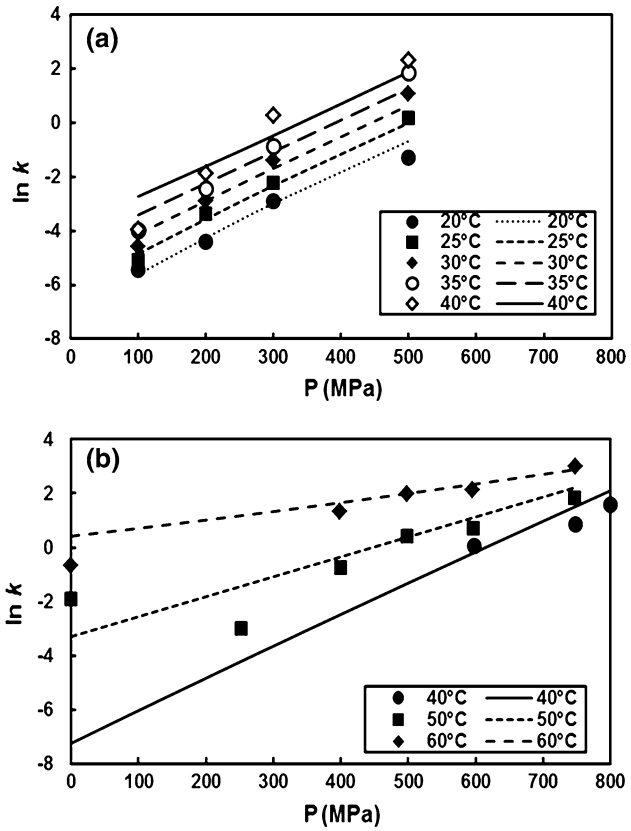

Fig. 5 Experimental (*symbols*) and predicted (*lines*) inactivation rate constants of orange juice PME inactivation with the Eyring–Arrhenius model. Data reported by **a** Plot generated from Katsaros et al. [52]; **b** Modified from Polydera et al. [90]

(600 MPa, 50 °C). The Eyring–Arrhenius parameters obtained by Polydera et al. [90] failed to consistently estimate $k(P, T)$ in the entire experimental range. Predictions of the kinetic rate constant were inaccurate at 100–250 MPa, but the model fit significantly improved in the proximity of the reference conditions selected (400–800 MPa, 40–60 °C).

Weemaes et al. [121] and van den Broeck et al. [112] encountered antagonistic pressure effects on k, since the enzyme was stabilized at pressures below 250–350 MPa for orange juice PME (Fig. 6) and also for avocado polyphenoloxidase (PPO). The Eyring relation (Eq. 43) was not constant throughout the tested pressure range, and both Weemaes et al. [121] and van den Broeck et al. [112] opted to apply an empirical model to estimate pressure dependence of k_{ref} (Eq. 48). Weemaes et al. [121] found that the activation energy decayed exponentially as the pressure system increased (Eq. 49), whereas van den Broeck et al. [112] reported a linear function for E_a (P) (Eq. 50).

$$\ln k_{\text{ref}}(P) = c_1 + c_2 \cdot P + c_3 \cdot P^2 + c_4 \cdot P^3 \quad (48)$$

$$E_{\text{a}}(P) = E_{\text{aP}} \cdot [\exp(-c_5 \cdot P)] \quad (49)$$

$$E_{\text{a}}(P) = c_5 - c_6 \cdot P \quad (50)$$

Table 5 Reported parameters for the secondary Eyring–Arrhenius-related models and its variants

Target	Medium	Pressure Come up time Holding time Depressurization Temperature	Kinetic model	Model parameters	Regression software	References
Alkaline phosphatase	Bovine milk	0.1–725 MPa 100 MPa min^{-1} 14–300 min NR 25–63 °C	Decimal reduction time empirical model (Eq. 72)	$c_1 = 3.33 \pm 0.16$ $c_2 = (3.88 \pm 0.77) * 10^{-3}$ $c_3 = (-1.05 \pm 0.09) * 10^{-5}$ $c_4 = 4.88 \pm 0.02$ $c_5 = (5.3 \pm 0.90) * 10^{-2}$ $c_6 = (-2.7 \pm 0.7) * 10^{-8}$ $T_{ref} = 323$ K	SAS	Ludikhuyze et al. [62]
Lactobacillus brevis	Orange juice Greek Valencia variety pH 3.8, 11.6°Brix	100–500 MPa NR 0–30 min NR 20–40 °C	Eyring–Arrhenius decimal reduction times (Eq. 68)	$D_{refP,T} = 3.42 \pm 0.51$ min^{-1} $P_{ref} = 300$ MPa $T_{ref} = 303$ K $z_T = 23.8 \pm 1.4$ °C $z_P = 94.7 \pm 7.8$ MPa $a = -0.009 \pm 0.001$ MPa^{-1}	SYSTAT 8.0 Least squares regression analysis	Katsaros et al. [52]
Lactobacillus plantarum	Orange juice Greek Valencia variety pH 3.8, 11.6°Brix	100–500 MPa NR 0–30 min NR 20–40 °C	Eyring–Arrhenius decimal reduction times (Eq. 68)	$D_{refP,T} = 1.32 \pm 0.11$ min^{-1} $P_{ref} = 300$ MPa $T_{ref} = 303$ K $z_T = 18.8 \pm 1.3$ °C $z_P = 95.0 \pm 11$ MPa $a = -0.013 \pm 0.002$ MPa^{-1}	SYSTAT 8.0 Least squares regression analysis	Katsaros et al. [52]
Lipoxygenase (LOX)	Tris–HCl buffer (0.01 M, pH 9) Commercial lyophilized soybean type B LOX	50–650 MPa 100 MPa min^{-1} NR NR 10–64 °C	Empirical Eyring–Arrhenius (Eq. 55)	$c_1 = -3.12 \pm 0.28$ $c_2 = (-1.39 \pm 0.18) * 10^{-1}$ $c_3 = (2.66 \pm 0.27) * 10^{-3}$ $c_4 = -15.6 \pm 1.4$ $c_5 = (7.1 \pm 0.28) * 10^{-2}$	SAS	Ludikhuyze [60, 61]
Pectinmethylesterase (PME)	Orange juice Greek Valencia variety pH 3.8, 11.6°Brix	100–500 MPa NR 0–30 min NR 20–40 °C	Eyring–Arrhenius (Eq. 47)	$k_{refP,T} = 0.582 \pm 0.048$ min^{-1} $P_{ref} = 300$ MPa $T_{ref} = 308$ K $E_{aP} = 95 \pm 11$ kJ mol^{-1} $V_T^{\neq} = -30 \pm 5$ cm^3 mol^{-1} $a = 0.64 \pm 0.07$ cm^3 mol^{-1} K^{-1} $g = -0.002 \pm 0.0003$ MPa^{-1}	SYSTAT 8.0 Least squares regression analysis	Katsaros et al. [52]

Table 5 continued

Target	Medium	Pressure Come up time Holding time Depressurization Temperature	Kinetic model	Model parameters	Regression software	References
Pectinmethylesterase (PME)	Orange juice Navel variety (*Citrus sinesis*)	100–800 MPa NR 0–30 min NR 30–60 °C	Eyring–Arrhenius (Eq. 47)	$k_{refP,T} = 1.76\ min^{-1}$ $P_{ref} = 600$ MPa $T_{ref} = 323$ K $E_{aP} = 148$ kJ/mol $V_T^{\neq} = -25.1\ cm^3 mol^{-1}$ $a = 0.703\ cm^3\ mol^{-1}\ K^{-1}$ $g = 8.374 \times 10^{-4}\ MPa^{-1}$ Valid in 40–60 °C range only due to enzyme reactivation at $T < 40$ °C[a]	SYSTAT	Polydera et al. [90]
Pectinmethylesterase (PME)	Deionized water (pH 4.5) Commercial orange peel PME 0.4 mg PME powder per ml of buffer	50–900 MPa NR 20–220 min NR 15–82 °C	Empirical Eyring–Arrhenius (Eq. 52)	$c_1 = -1.88 \pm 0.10$ $c_2 = (-17.55 \pm 1.09) * 10^{-3}$ $c_3 = (53.27 \pm 3.26) * 10^{-6}$ $c_4 = (-35.95 \pm 2.79) * 10^{-9}$ $c_5 = 352.12 \pm 18.55$ $c_6 = 0.348 \pm 0.027$	NR	Van den Broeck et al. [112]
Pectinmethylesterase (PME)	Citric acid buffer 5 mM, pH 3.7 Lyophilized orange pulp PME extract Navel variety 2.0 mg PME powder per ml of buffer	50–900 MPa NR 20–220 min NR 15–82 °C	Empirical Eyring–Arrhenius (Eq. 52)	$c_1 = -2.39 \pm 0.17$ $c_2 = (-19.00 \pm 1.83) * 10^{-3}$ $c_3 = (55.20 \pm 5.94) * 10^{-6}$ $c_4 = (-38.50 \pm 5.35) * 10^{-9}$ $c_5 = 193.44 \pm 22.89$ $c_6 = 0.248 \pm 0.036$	NR	Van den Broeck et al. [112]
Polyphenoloxidase (PPO)	Phosphate buffer (pH 7; 0.1 M) Lyophilized avocado PPO powder 0.5 mg PPO powder per ml of buffer	0.1–900 MPa NR 35–180 min NR 25–77.5 °C	Empirical Eyring–Arrhenius (Eq. 51)	$c_1 = -2.42 \pm 0.07$ $c_2 = (-17.2 \pm 0.7) * 10^{-3}$ $c_3 = (41.1 \pm 1.8) * 10^{-6}$ $c_4 = (-23.3 \pm 1.3)\ * 10^{-9}$ $c_5 = (-16.8 \pm 0.6) * 10^{-4}$ $E_{aP} = 342.30 \pm 11.63\ kJ\ mol^{-1}$	NR	Weemaes et al. [121]
Saccharomyces cerevisae	0.85 % NaCl solution 8.0×10^6–1.0×10^7 cfu ml^{-1} inoculum at stationary phase IFO 0234 strain	120–300 MPa 2 min 0–40 min 30 s (−20) to 50 °C	Quadratic model (Eq. 70)	$c_1 = -4.26$ $c_2 = 1.25 * 10^{-2}$ $c_3 = -3.37 * 10^{-2}$ $c_4 = 8.55 * 10^{-6}$ $c_5 = -7.55 * 10^{-5}$ $c_6 = 1.42 * 10^{-3}$ $P_{ref} = 0.1$ MPa $T_{ref} = 273$ K	NR	Hashizume et al. [42]

Table 5 continued

Target	Medium	Pressure Come up time Holding time Depressurization Temperature	Kinetic model	Model parameters	Regression software	References
Zygosaccharomyces bailii	Tris–HCl buffer 40 mM, pH 6.5 CBS 109	120–320 MPa 100 MPa min^{-1} 0–60 min NR (−5) to 45 °C	Reduced quadratic model (Eq. 71)	$c_1 = 1.55 \pm 0.04$ $c_2 = -(15.05 \pm 0.49) * 10^{-3}$ $c_3 = -(24.05 \pm 1.53) * 10^{-3}$ $c_4 = (23.52 \pm 6.63) * 10^{-6}$ $c_5 = -(16.42 \pm 1.01) * 10^{-4}$ $P_{ref} = 220$ MPa $T_{ref} = 293$ K	SAS	Reyns et al. [97]

[a] The Eyring-Arrhenius model parameters obtained by Polydera et al. [90] are valid only for the 40–60 °C range, since large deviations occur at lower temperature

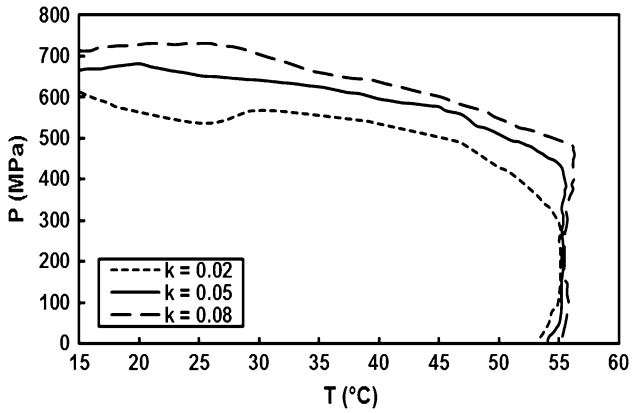

Fig. 6 Pressure-–temperature isorate inactivation constant contour plots for PME extracted from orange and suspended in citric acid buffer (5 mM, pH 3.7), modified from Van den Broeck et al. [112]

The substitution of E_a (P) and k_{ref} (P) in the Arrhenius equation (Eq. 44) yields two empirical models describing the effects of pressure and temperature on k (Eqs. 51–52). Empirical parameters c_1–c_4 describe the effect of pressure on k_{ref}, and the calculated values for PPO [121] and PME [112] are very similar (Table 5).

$$k = \exp\left\{c_1 + c_2 \cdot P + c_3 \cdot P^2 + c_4 \cdot P^3 + \left[-\frac{E_{aP} \cdot [\exp(-c_5 \cdot P)]}{R}\left(\frac{1}{T} - \frac{1}{T_{ref}}\right)\right]\right\} \quad (51)$$

$$k = \exp\left\{c_1 + c_2 \cdot P + c_3 \cdot P^2 + c_4 \cdot P^3 + \left[-\frac{c_5 - c_6 \cdot P}{R}\left(\frac{1}{T} - \frac{1}{T_{ref}}\right)\right]\right\} \quad (52)$$

Conversely, Ludikhuyze et al. [60, 61] found that elevating pressure increased the inactivation rates at all temperatures, and therefore, the Eyring model (Eq. 43) was valid for lipoxygenase (LOX) inactivation at 50–800 MPa and 10–64 °C. Antagonistic effects for combined pressure–temperature treatments were again present for the low-temperature ($T < 40$ °C) and high-pressure ($P > 475$ MPa) region, and minimum values were registered between 30 and 40 °C. In this case, the Arrhenius model (Eq. 44) could not be applied as denoted by the calculated E_a values, which were negative for $T < 40$ °C and positive for $T > 40$ °C. Therefore, Ludikhuyze et al. [60] elaborated an empirical model for k_{ref} (T) (Eq. 53) and $\Delta V^{\neq}$ (T) (Eq. 54). The incorporation of Eqs. 53 and 54 into the Eyring equation resulted in an Eyring empirical secondary model (Eq. 55).

$$\ln k_{ref}(T) = c_1 + c_2 \cdot T + c_3 \cdot T^2 \quad (53)$$

$$\Delta V^{\neq}(T) = c_4 \cdot T \cdot [\exp(-c_5 \cdot T)] \quad (54)$$

$$\ln k = c_1 + c_2 \cdot T + c_3^2 \cdot T - \left\{ \frac{c_4 \cdot T \cdot [\exp(-c_5 \cdot T)]}{R \cdot T} \cdot (P - P_{\text{ref}}) \right\} \quad (55)$$

Doona et al. [32] predicted the processing time ($t_p = 1/k$) required to achieve 6-log reductions in *L. monocytogenes* as a function of pressure and temperature with empirical models based on the Eyring and the Arrhenius equations. The pressure dependence of ln k was not linear, and the authors decided to include the effect of pressure on $\Delta V^{\neq}$, given by the compressibility factor $\Delta\beta$ and defined through Eqs. 56–58 [32, 73, 113].

$$\Delta\beta = \left(\frac{\partial \Delta V^{\neq}}{\partial P}\right)_T = -R \cdot T \cdot \left(\frac{\partial^2 \ln k}{\partial P^2}\right)_T \quad (56)$$

$$\left(\frac{\partial \ln k}{\partial P}\right)_T = -\frac{1}{R \cdot T} \cdot \left[\Delta\beta \cdot (P - P_{\text{ref}}) + \Delta V^{\neq}\right] \quad (57)$$

$$\ln k = \ln k_{\text{ref}} - \frac{\Delta V^{\neq} \cdot (P - P_{\text{ref}})}{R \cdot T} + \frac{\Delta\beta \cdot (P - P_{\text{ref}})^2}{2 \cdot R \cdot T} \quad (58)$$

Furthermore, the extended Eyring model (Eq. 56) was reparametrized by defining t_p, γ as in Eq. (59–60), $P_{\text{ref}} = 6.98$ MPa ($\approx$1 kpsi), and regrouping all terms (Eq. 61–64) to yield a linear quadratic equation with three parameters (Eq. 63). Similar modifications were performed for the Arrhenius equation (model not shown), and the temperature dependence of t_p was modeled with a nondimensional linear first-order equation. Doona et al. [32] reported that both of the secondary models accurately predicted t_p for a new set of experimental under isothermal or isobaric conditions.

$$\gamma = \frac{1}{P_{\text{ref}}} \cdot (P - P_{\text{ref}}) = \frac{P}{P_{\text{ref}}} = 1 + \gamma \quad (59)$$

$$t_p = \frac{1}{k} \quad (60)$$

$$k = A \cdot \exp(-c_1 \cdot \gamma) \cdot \exp(-c_2 \cdot \gamma^2) \quad (61)$$

$$A = k_{\text{ref}} \cdot \exp\left[-\left(\frac{\Delta V^{\neq} \cdot P_{\text{ref}}}{R \cdot T} - \frac{\Delta\beta \cdot P_{\text{ref}}^2}{2 \cdot R \cdot T}\right)\right]; c_0 = \ln\frac{1}{A} \quad (62)$$

$$c_1 = \frac{\Delta V^{\neq} \cdot P_{\text{ref}}}{R \cdot T} - \frac{\Delta\beta \cdot P_{\text{ref}}^2}{R \cdot T} \quad (63)$$

$$c_2 = -\frac{\Delta\beta \cdot P_{\text{ref}}^2}{2 \cdot R \cdot T} \quad (64)$$

$$\ln t_p = c_0 + c_1 \cdot \gamma - c_2 \cdot \gamma^2 \quad (65)$$

For microbial inactivation, Katsaros et al. [52] modified Eqs. 43 and 44 by defining $k(T)$ and $k(P)$ as a function of decimal reduction times of *Lactobacillus brevis* and *Lactobacillus plantarum* in orange juice at reference conditions (D_{Tref}, D_{Pref}) and parameters z_T and z_P as in Eqs. 66 and 67.

$$\frac{k}{k_{T_{\text{ref}}}} = \frac{D_{T_{\text{ref}}}}{D_T \cdot 10^{\left(\frac{T_{\text{ref}} - T}{z_T}\right)}} \quad (66)$$

$$\frac{k}{k_{P_{\text{ref}}}} = \frac{D_{P_{\text{ref}}}}{D_P \cdot 10^{\left(\frac{P_{\text{ref}} - P}{z_P}\right)}} \quad (67)$$

Both k (T) and k (P) were associated by assuming an Arrhenius-type relationship and an expression relating decimal reduction time (D) with the processing conditions P and T (Eq. 68).

$$D = D_{P_{\text{ref}}T_{\text{ref}}} \cdot \exp\left\{(P - P_{\text{ref}}) \cdot \left[\frac{\Delta V^{\neq}(T)}{R \cdot T} + \frac{2.303}{z_P}\right] + 2.303\frac{(T - T_{\text{ref}})}{z_T} + \frac{E_a(P)}{RT} \cdot \left(\frac{1}{T} - \frac{1}{T_{\text{ref}}}\right)\right\} \quad (68)$$

Katsaros et al. [52] reported a good fit for predicted k (P, T) of *L. brevis* and *L. plantarum* in orange juice ($R^2 = 0.951$ and 0.977, respectively) inactivation in the 100–500 MPa and 20–40 °C range. Pressure resistance at the reference temperature was almost the same for *L. brevis* ($z_P = 94.7 \pm 7.8$ MPa) and *L. plantarum* ($z_P = 95.0 \pm 11$ MPa). Nonetheless, thermal sensibility was lower for the former ($z_T = 23.8 \pm 2.4$ °C) than for the latter ($z_T = 23.8 \pm 2.4$ °C and the decimal reduction time at reference conditions was 2.1 min higher (Table 5).

Although decimal reduction times for the inactivation of enzymes are rarely reported, Ludikhuyze et al. [62] attempted to fit the Bigelow model (Eq. 28) to the inactivation of raw bovine milk alkaline phosphatase (0.1–700 MPa; 25–63 °C). Enzyme activity kinetics followed a first-order kinetics, and therefore, k was related to decimal reduction times as in Eqs. (66–67). Adverse effects of PATP were once again present for the low-pressure/high-temperature region, and the pressure-dependent terms (Eq. 67) were not valid in the experimental range tested. Ludikhuyze et al. [62] opted to fit experimental D (T, P) values to the empirical model shown in Eq. 69 (Table 5) and reported that 95 % of the predicted data points showed less than 15 % of error when compared to the experimental values. Parameter c_1 could represent D_T at a reference temperature, and the calculated value at $T_{\text{ref}} = 50$ °C was $D_T = 3.33$ min (Table 5), implying that alkaline phosphatase has an elevated thermal resistance.

$$\log_{10} D(P,T) = c_1 + c_2 \cdot P + c_3 \cdot P^2 - \frac{T - T_{\text{ref}}}{c_4 + c_5 \cdot P + c_6 \cdot P^2} \quad (69)$$

Hashizume et al. [42] studied the effect of high pressure (120–300 MPa) and sub-zero temperatures (−20 to 50 °C) on *S. cerevisae* inactivation. Inactivation kinetics apparently followed first-order kinetics at all temperatures, whereas

pressures below 180 MPa and temperatures between 0 and 40 °C caused only a minor microbial inactivation. A quadratic model (Eq. 70) was utilized to predict k as a function of both pressure and temperature. The isokinetic rate diagrams for *S. cerevisae* inactivation presented an elliptical trend similar to a protein denaturation diagram [45, 69, 117]. Hashizume et al. [42] concluded that the resemblance of microbial and enzymatic isorate contours may be due to the adverse effects of HPP on key enzymatic processes of microorganisms. Furthermore, Reyns et al. [97] demonstrated statistically a slightly improved prediction of decimal reduction times for *Zygosaccharomyces bailii* when the linear pressure–temperature term, denoted by $(P - P_{ref})$-$(T - T_{ref})$, was omitted (Eq. 71). The values for the parameters of Eqs. 70 and 71 are shown in Table 5.

$$\log_{10} k(P,T) = c_1 + c_2 \cdot (P - P_{ref}) + c_3 \cdot (T - T_{ref}) + c_4 \cdot (P - P_{ref})^2 + c_5 \cdot (P - P_{ref}) \cdot (T - T_{ref}) + c_6 \cdot (T - T_{ref})^2 \quad (70)$$

$$\log_{10} D(P,T) = c_1 + c_2 \cdot (P - P_{ref}) + c_3 \cdot (T - T_{ref}) + c_4 \cdot (P - P_{ref})^2 \quad + c_5 \cdot (T - T_{ref})^2 \quad (71)$$

Even though there are other empirical pressure–temperature secondary models, care must be taken when using them since most lack generality and have validity only for the specific inactivation study for which the equation was developed. Additionally, most of these polynomial parameters also lack a comprehensible biological or physical basis and may include severe and numerous slope changes over a wide range leading to incorrect estimations of kinetics parameters.

Thermodynamic Model

Hawley [43] developed a purely thermodynamic model to describe ΔG for the reversible pressure–temperature denaturation of chymotrypsinogen at 0.1–700 MPa and 8.5–70 °C. By integrating the general free Gibbs energy equation (Eq. 72), and including the compressibility factor (β), thermal expansivity (α), and specific heat (C_p) contribution with the Maxwell relations, the result is the model proposed by Hawley [43] shown below (Eq. 73):

$$d(\Delta G) = -\Delta S \mathrm{d}T + \Delta V \mathrm{d}P \quad (72)$$

$$\Delta G = \frac{\Delta\beta}{2} \cdot (P - P_{ref})^2 + \Delta\alpha \cdot (P - P_{ref}) \cdot (T - T_{ref}) - \Delta C_p \left[T \left(\ln \frac{T}{T_{ref}} - 1 \right) + T_{ref} \right] + \Delta V_{ref} \cdot (P - P_{ref}) - \Delta S_{ref} \cdot (T - T_{ref}) + \Delta G_{ref} \quad (73)$$

Eq. 73 could be incorporated into the model that relates the equilibrium constant ($K^{\neq}$) between the reactants and the activated complex with the chemical reaction constant k described by the Transitional State Theory (See the *Pressure Thermodynamics Fundamentals* section) and the general ΔG equilibrium model (Eq. 72). The combination of Eqs. 72–74 yields the thermodynamic kinetic model (Eq. 75) [34, 63, 73, 121]:

$$\Delta G = -R \cdot T \cdot \ln K \quad (74)$$

$$\ln k = \frac{\Delta\beta}{2 \cdot R \cdot T} \cdot (P - P_{ref})^2 + \frac{\Delta V_{ref}^{\neq}}{R \cdot T} \cdot (P - P_{ref}) - \frac{\Delta S_{ref}}{R \cdot T} \cdot (T - T_{ref}) + \frac{\Delta\alpha}{R \cdot T} (P - P_{ref}) \cdot (T - T_{ref}) - \frac{\Delta C_p}{R \cdot T} \cdot \left\{ T \cdot \left[\ln \left(\frac{T}{T_{ref}} \right) - 1 \right] + T_{ref} \right\} + \ln k_{ref} \quad (75)$$

The thermodynamic kinetic model accurately fit experimental k values for the inactivation of soybean lipoxygenase (LOX) in Tris–HCl buffer [48], green pea juice, and intact green peas [49] over wide pressure–temperature ranges (Table 6). Weemaes et al. [121] rejected this kinetic model (Eq. 75) for the case of PME inactivation because the statistical analysis showed that the residuals for k as a function of pressure were not randomly distributed. Weemaes et al. [121] stated that Eq. 75 could not be applied for avocado PPO inactivation because Hawley [43] originally developed the thermodynamic model to describe the *reversible* inactivation of chymotrypsinogen. The authors concluded that *irreversible* enzyme inactivation mechanisms differ from those for *reversible* inactivation, and therefore, a different mathematical model to estimate $k(P, T)$ should be used.

In addition, the thermodynamic model proposed by Hawley [43] assumes that thermophysical parameters ΔC_p, $\Delta\alpha$, and $\Delta\beta$ remain constant for all pressure and temperature values, which may not always be the case [103]. The general ΔG equation (Eq. 70) could be approximated using a Taylor expansion series (Eq. 76) where the additional third-degree terms would represent the pressure and temperature dependence of ΔC_p, $\Delta\alpha$, and $\Delta\beta$ [9, 18, 45, 103].

$$\Delta G = \Delta G_{ref} + \Delta V_{ref} \cdot (P - P_{ref}) - \Delta S_{ref} \cdot (T - T_{ref}) + \frac{\Delta\beta}{2} \cdot \Delta V_{ref} \cdot (P - P_{ref})^2 + \Delta\alpha \cdot (P - P_{ref}) \cdot (T - T_{ref}) - \frac{\Delta C_p}{2 \cdot T_{ref}} \cdot (T - T_{ref})^2 \quad (76)$$

Ly-Nguyen et al. [66] incorporated additional polynomial degree terms given by the Taylor expansion series (Eq. 77), and the distortion of the elliptical trend of the isorate contour plot reported by other authors was also observed [9, 103].

$$\frac{\Delta\beta_2}{2 \cdot R \cdot T} \cdot (P - P_{ref})^3 + \frac{\Delta C_{p^2}}{2 \cdot R \cdot T \cdot T_{ref}} \cdot (T - T_{ref})^3 + \frac{2 \cdot \Delta\alpha_2}{R \cdot T} \cdot (P - P_{ref})^2 \cdot (T - T_{ref}) \quad (77)$$

Table 6 Reported parameters for the secondary Hawley thermodynamic model and its variants

Target	Medium	Pressure Come up time Holding time Depressurization Temperature	Kinetic model	Model parameters	Regression software	References
Chymotrypsinogen	Aqueous solution, pH 2.07	0.1–700 MPa NR NR NR 8.5–70 °C	Thermodynamic model (Eq. 73)	$\Delta\beta = -0.296$ cm^6 J^{-1} mol^{-1} $\Delta V^{\neq}_{ref} = -14.3$ cm^3 mol^{-1} $\Delta S_{ref} = 950$ J mol^{-1} K^{-1} $\Delta\alpha = 1.32$ cm^3 mol^{-1} K^{-1} $\Delta C_p = 15{,}900$ J mol^{-1} ln $k_{ref} = -4.66$ $P_{ref} = 0.1$ MPa $T_{ref} = 273$ K Calculated from reported ΔG_0[a]	NR	Hawley [43]
Lipoxygenase (LOX)	Green pea juice	0.1–625 MPa 100–125 MPa min^{-1} 0.1–625 MPa NR −15 to 70 °C	Thermodynamic model (Eq. 75)	$\Delta\beta = -(0.0937 \pm 0.0192)$ cm^6 J^{-1} mol^{-1} $\Delta V^{\neq}_{ref} = -(38.18 \pm 3.37)$ cm^3 mol^{-1} $\Delta S_{ref} = 13.79 \pm 11.78$ J mol^{-1}K^{-1} $\Delta\alpha = -(0.12 \pm 0.09)$ cm^3 mol^{-1}K^{-1} $\Delta C_p = 1{,}837.4 \pm 244.0$ J mol^{-1} ln $k_{ref} = -3.71$ $P_{ref} = 500$ MPa $T_{ref} = 298$ K	SAS	Indrawati et al. [49]
Lipoxygenase@(LOX)	Green pea	0.1–625 MPa 100–125 MPa min^{-1} 0.1–625 MPa NR −10 to 70 °C	Thermodynamic model (Eq. 75)	$\Delta\beta = -(0.1382 \pm 0.0406)$ cm^6 J^{-1} mol^{-1} $\Delta V^{\neq}_{ref} = -(50–76 \pm 7.37)$ cm^3 mol^{-1} $\Delta S_{ref} = 21.19 \pm 25.69$ J mol^{-1} K^{-1} $\Delta\alpha = -(0.23 \pm 0.20)$ cm^3 mol^{-1} K^{-1} $\Delta C_p = 1{,}058.6 \pm 375.0$ J mol^{-1} ln $k_{ref} = -2.85$ $P_{ref} = 500$ MPa $T_{ref} = 298$ K	SAS	Indrawati et al. [49]
Lipoxygenase@(LOX)	Tris–HCl buffer 0.1 M, pH 9 Lyophilized soybean LOX powder 0.4 mg enzyme powder per ml of buffer	0.1–625 MPa 100–125 MPa min^{-1} 0.1–625 MPa NR −10 to 70 °C	Thermodynamic model (Eq. 75)	$\Delta\beta = -(0.1382 \pm 0.0406)$ cm^6 J^{-1} mol^{-1} $\Delta V^{\neq}_{ref} = -(50–76 \pm 7.37)$ cm^3 mol^{-1} $\Delta S_{ref} = 21.19 \pm 25.69$ J mol^{-1} K^{-1} $\Delta\alpha = -(0.23 \pm 0.20)$ cm^3 mol^{-1} K^{-1} $\Delta C_p = 1{,}058.6 \pm 375.0$ J mol^{-1} ln $k_{ref} = -2.85$ $P_{ref} = 0.5$ MPa $T_{ref} = 298$ K	SAS	Indrawati et al. [48]

Table 6 continued

Target	Medium	Pressure Come up time Holding time Depressurization Temperature	Kinetic model	Model parameters	Regression software	References
Pectinmethylesterase (PME)	Tris–HCl buffer 20 mM, pH 7.0 Carrot PME extract	100–825 MPa 100 MPa min^{-1} 0–250 min NR 10–65 °C	Thermodynamic model (Eq. 75)	$\Delta\beta = -(1.40 \pm 1.06)$ cm^6 J^{-1} mol^{-1} $\Delta V^{\neq}_{ref} = -(341.95 \pm 22.21)$ cm^3 mol^{-1} $\Delta S_{ref} = -20.65 \pm 7.20$ J mol^{-1} K^{-1} $\Delta\alpha = 3.20 \pm 0.26)$ cm^3 mol^{-1} K^{-1} $\Delta C_p = 3{,}046.6 \pm 207.2$ J mol^{-1} ln $k_{ref} = -4.36$ $P_{ref} = 700$ MPa $T_{ref} = 323$ K	NR	Ly-Nguyen et al. [66]
Pectinmethylesterase (PME)	Tris–HCl buffer 20 mM, pH 7.0 Carrot PME extract	100–825 MPa 100 MPa min^{-1} 0–250 min NR 10–65 °C	Extended thermodynamic model (Eq. 76, 77)	$\Delta\beta = -(0.0307 \pm 0.03467)$ cm^6 J^{-1} mol^{-1} $\Delta V^{\neq}_{ref} = -(41.64 \pm 2.70)$ cm^3 mol^{-1} $\Delta S_{ref} = 148.3 \pm 24.01$ J mol^{-1} K^{-1} $\Delta\alpha = -(0.0415 \pm 0.0967)$ cm^3 mol^{-1} K^{-1} $\Delta C_p = 4{,}573.9 \pm 1306.7$ J mol^{-1} ln $k_{ref} = -2.70$ $\Delta\beta_2 = -(0.00012 \pm 0.00004)$ [cm^6 J^{-1} mol^{-1}]^2 $\Delta\alpha_2 = 0.00026 \pm 0.00015$ [cm^3 mol^{-1} K^{-1}]^2 $\Delta C_{p2} = 88.02 \pm 28.94$[J mol^{-1}]^2 $P_{ref} = 700$ MPa $T_{ref} = 323$ K	NR	Ly-Nguyen et al. [66]
Polygalacturonase (PG)	Sodium acetate buffer 40 mM, pH 4.4 Tomato PG extract	300–600 MPa 100 MPa min^{-1} 0–200 min NR 5–50 °C	Reduced thermodynamic model (Eq. 78)	$\Delta V^{\neq}_{ref} = -(55.69 \pm 2.95)$ cm^3 mol^{-1} $\Delta S_{ref} = 265.28 \pm 18.14$ J mol^{-1} K^{-1} $\Delta\alpha = -(1.029 \pm 0.15)$ cm^3 mol^{-1} K^{-1} ln $k_{ref} = -3.26$ $P_{ref} = 400$ MPa $T_{ref} = 298$ K	SAS	Fachin et al. [34]

[a] Hawley [43] used ΔG and ΔG_0 instead of ln$k$ and lnk_{ref} in the thermodynamic model nomenclature (Eq. 73)

The addition of these higher-order terms yielded a better fit ($R^2 = 0.941$) than the original Hawley model ($R^2 = 0.891$) for carrot PME inactivation in the 100–825 MPa and 10–65 °C range [66]. Antagonistic pressure–temperature effects were observed as the value of ln k decreased, particularly at 50–65 °C and 100–300 MPa (Fig. 7). Apparently, the inactivation rate values increased exponentially until reaching the high-pressure (600–800 MPa), low-temperature region (10–40 °C), where an asymptotic trend was observed (Fig. 7a, b). For moderate temperatures (50–65 °C), the antagonistic effects were clearly noticeable in the 100–400 MPa region. The second-order thermodynamic model (Eq. 76) failed to adjust to the lower experimental k values (Fig. 7c, d).

Another modification of the thermodynamic model (Eq. 75) was proposed by Fachin et al. [34] who noted that the isorate contour plots for different pressure–temperature combinations displayed no elliptical trend for the tomato PG inactivation kinetics. Consequently, the compressibility factor (β) and the specific heat capacity (C_p) from the thermodynamic model were removed (Eq. 78) because the authors stated that these terms are related to the elliptical trend. Fachin et al. [34] found a satisfactory correlation ($R^2 = 0.92$) between experimental data and estimated k (P, T) values using the reduced thermodynamic model (Eq. 76). However, the kinetic study on the inactivation of tomato PG covered a narrower pressure–temperature range (300–600 MPa, 5–50 °C) as compared to the other HPP enzyme inactivation cases presented in Table 6. Therefore, the pressure and temperature range used by these authors may have affected the shape of the isorate contour plots.

$$\ln k = \frac{\Delta V^{\neq}_{\text{ref}}}{R \cdot T} \cdot (P - P_{\text{ref}}) - \frac{\Delta S_{\text{ref}}}{R \cdot T} \cdot (T - T_{\text{ref}}) + \frac{\Delta \alpha}{R \cdot T} \cdot (P - P_{\text{ref}}) \cdot (T - T_{\text{ref}}) + \ln k_{\text{ref}} \quad (78)$$

The thermodynamic model can simultaneously describe pressure and temperature effects on the inactivation rate constants with a solid theoretical background that can be interpreted physically. Most importantly, a thermodynamic model can describe experimental data with antagonistic pressure–temperature effects while still yielding accurate predictions [48, 49, 66]. However, the large number of parameters involved implies an extensive experimental plan covering a wide pressure–temperature range, which makes them potentially impractical to use [48, 66, 73].

Simultaneous Pressure and Temperature Effects on Weibull Model Parameters

Peleg et al. [84] questioned the application of the Arrhenius model to describe the temperature effect on inactivation

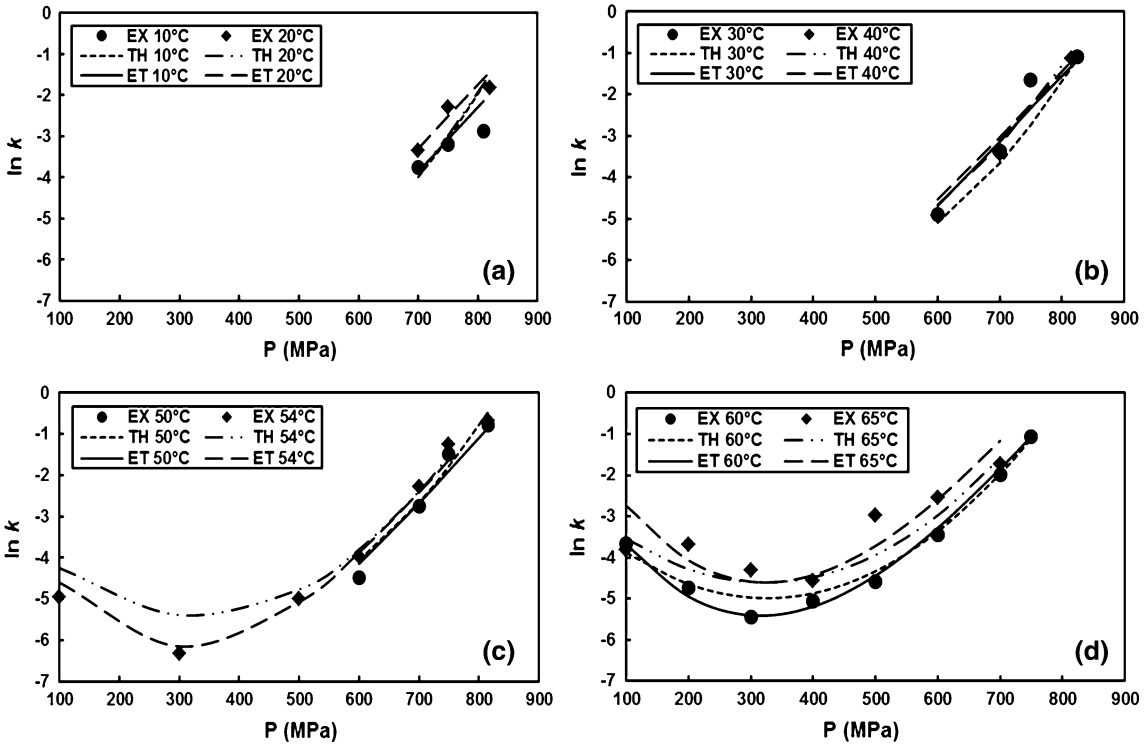

Fig. 7 Experimental (EX) and predicted values of the kinetic rate constant (k) as a function of pressure and temperature for carrot PME inactivation with the thermodynamic (TH; Eq. 76) and the extended thermodynamic model (ET; Eqs. 76–77). Plots generated from Ly-Nguyen et al. [66]

kinetics, arguing the existence of temperature regions where the reaction system remains inert. The authors cited as an example oxidation and browning reactions, which become significant only when the temperature is increased. On the other hand, the parameters b' and n of the Weibull power law model are not necessarily constant and depend on the pressure and temperature condition applied [86]. Peleg et al. [84] suggested a log-logistic model to simulate null reaction rates for low-temperature regions, and a subsequent increase beyond a critical temperature level (T_c). Corradini et al. [22] applied the log-logistic model to describe the Weibull rate parameter b' as a function of temperature (Eq. 79).

$$b'(T) = \ln\{1 + \exp[w_T(T - T_c)]\}^m \quad (79)$$

The parameter T_c denotes the temperature at which $b'(T)$ increases linearly for $m = 1$. If $T > T_c$, the parameter $b'(T)$ increases to the power $w_T(T - T_c)$, where w_T determines the rate at which $b'(T)$ increases with temperature. Conversely, when $T < T_c$, the exponential term tends to zero and $b'(T)$ is approximately ln (1) = 0. This model may be applied also for high-pressure inactivation (Eq. 80) under isothermal conditions [23, 86].

$$b'(P) = \ln\{1 + \exp[w_P(P - P_c)]\}^m \quad (80)$$

Pressure and temperature increases are expected to lower parameters T_c and P_c (Eqs. 81–82) since inactivation should be favored by more severe treatments [85]. However, these exponential-logistic models may not accurately predict antagonistic pressure–temperature effects as in the case of PME.

$$P_c(T) = P_{c_0} \cdot \exp(-w_1 \cdot T) \quad (81)$$

$$T_c(P) = T_{c_0} \cdot \exp(-w_2 \cdot P) \quad (82)$$

The pressure effect on the parameter b' may be expressed also using the Bigelow model (Eq. 83) as reported by Pilavtepe-Çelik et al. [89] or as a simple linear model as shown in Eq. 84 [15].

$$\log_{10} b' = \log_{10} b'_{ref} - \left(\frac{P - P_{ref}}{z}\right) \quad (83)$$

$$b' = \text{slope} + \text{intercept} \quad (84)$$

The shape parameter n of the Weibull inactivation model (Eq. 9) has often been reported to display a slight or no temperature dependence [11, 110]. This statement can sometimes be assumed for $n(P)$ as Chen and Hoover [15] did at certain pressure ranges for *Y. enterocolitica* ATCC 35669 inactivation kinetics in milk and sodium phosphate buffer. No significant differences were found for n in the 300–400 and 400–500 MPa regions for *Y. enterocolitica* inactivation in phosphate buffer and milk, respectively, so the mean value of n was applied for each pressure range. However, the former assumption that n is pressure-independent was not valid for the entire experimental pressure range (300–500 MPa). On the contrary, Doona et al. [31] and Buzrul and Alpas [10] observed concavity changes (Table 2), where n tended to increase with processing pressure temperature. Therefore, a constant $n(T)$ or $n(P)$ may not be the reflect of a nonsignificant pressure and/or temperature effect on the kinetic model parameters, but a consequence of the narrow pressure and temperature ranges under which the experiments were performed. The pressure dependence of the shape parameter, $n(P)$, can be calculated empirically, e.g., using the model proposed by Pilavtepe-Çelik et al. [89] for the inactivation of pathogens in carrot juice and peptone water (Eq. 85). The exponential model describing $P_c(T)$ and $T_c(P)$ (Eqs. 81–82) can also be applied to the model parameter $n(T)$ or $n(P)$ (Eqs. 86–87) [31].

$$n(P) = n_{ref} + a \cdot \left(\frac{1}{P} - \frac{1}{P_{ref}}\right) \quad (85)$$

$$n(P) = d_{0P}(T) \cdot \exp[-d_{1P}(T) \cdot P] \quad (86)$$

$$n(T) = d_{0T}(P) \cdot \exp[-d_{1T}(P) \cdot T] \quad (87)$$

Recently, Carreño et al. [13] proposed an alternative Weibull secondary model for the survival fraction ($\log_{10}S$) under isothermal and isobaric conditions by inferring that the pressure and temperature resistance of microorganisms followed a Weibull distribution. Pressure and temperature substituted the independent variable time (t) in Eq. 9 and resulted in Eqs. 88 and 89.

$$S(P) = -\left(\frac{P}{f_P}\right)^n \quad (88)$$

$$S(T) = -\left(\frac{T}{f_T}\right)^n \quad (89)$$

The parameters f_P and f_T represent the pressure and temperature for the first decimal reduction in the microbial population. The use of the isothermal model to describe the inactivation of *L. plantarum* at 0–400 MPa for 10–60 s in tangerine juice with an initial temperature of 15–45 °C yielded $R^2 = 0.952$–0.990 and $A_f = 1.021$–1.066 [13]. Although no sigmoidal curves were observed, Carreño et al. [13] also investigated the kinetics of *L. plantarum* HPP inactivation combined with mild heat treatments (45–90 °C, 10 s). The survival curves presented concavity changes, and the single Weibull model with pressure and temperature as independent variables (Eqs. 88–89) had an inaccurate fit (36 % prediction error). As a result, a biphasic Weibull model (Eq. 90) combining Eqs. 15 and 88 was applied and yielded a 9 % prediction error with $A_f = 1.009$.

$$N(T) = \frac{N_0}{1 + 10^{\Psi}}\left[10^{\left[\Psi - \left(\frac{T}{fT_1}\right)^{n_1}\right]} + 10^{-\left(\frac{T}{fT_2}\right)^{n_2}}\right] \quad (90)$$

Table 7 Reported simultaneous effect of pressure and temperature on the Weibull model parameters that describe PATP kinetics

Target	Medium	Pressure Come up time Holding time Depressurization Temperature	Kinetic model	Model parameters	Regression software	References
Escherichia coli	Peptone water 0.1 %, pH 6.95 10^7 cfu ml^{-1} O157:H7 933 strain Stationary phase	200–400 MPa 400 MPa min^{-1} 5–40 min >20 s 40 °C	Weibull parameter *n* inverse (Eq. 85)	$n_{ref} = 0.4 \pm 0.08$ $a = 125.5 \pm 10.2$ MPa	SigmaPlot 2000 v. 6.00	Pilavtepe-Çelik et al. [89]
Escherichia coli	Whey protein surrogate food system ATCC 11229 strain	207–439 MPa NR 0–300 min NR 30, 40, 50 °C	Weibull (Eqs. 80–86)	$P_c = 357$–458 MPa (30–50 °C) $w_P = 0.026$–0.042 1/MPa (30–50 °C) $d_{0P} = 5.7$–43.3 (30–50 °C) $d_{1P} = 0.00039$–0.00077 (30–50 °C)	NR	Doona et al. [31]
Lactobacillus plantarum	Fresh clementine mandarin (*Citrus reticula*, variety *Nules*) juice 2x10^8 cfu ml^{-1} inoculum	0–450 MPa 90 s 10–60 s 15 s 15, 30, 45 °C (initial)	Pressure-dependent Weibull biphasic model (Eq. 91)	$f_P = 128$–335 MPa (15–45 °C) $n = 2.41$–7.55 (15–45 °C)	Statgraphics Centurion XV	Carreño et al. [13]
Lactobacillus plantarum	Mandarin juice Clementine mandarin (*Citrus reticula*, commercial variety *Nules*) Fresh juice 2x10^8 cfu ml^{-1} inoculum	0–450 MPa 90 s 10–60 s 15 s 15, 30, 45 °C (initial)	Pressure-dependent Weibull biphasic model (Eq. 91)	$\Psi = 2.56$–3.08 (15–45 °C) $f_{P1} = 128$–335 MPa (15–45 °C) $f_{P2} = 445$–668 MPa (15–45 °C) $n = 3.28$–6.00 (15–45 °C)	Statgraphics Centurion XV	Carreño et al. [13]
Staphylococcus aureus	Carrot juice (pH 6.22) Fresh, squeezed juice 10^7 cfu ml^{-1} 485 strain Stationary phase	200–400 MPa 400 MPa min^{-1} 5–40 min >20 s 40 °C	Weibull parameter *n* inverse (Eq. 85)	$n_{ref} = 0.6 \pm 0.1$ $a = 230.4 \pm 65.4$ MPa	SigmaPlot 2000 6.00	Pilavtepe-Çelik et al. [89]
Staphylococcus aureus	Peptone water 0.1 %, pH 6.95 10^7 cfu ml^{-1} 485 strain Stationary phase	200–400 MPa 400 MPa min^{-1} 5–40 min >20 s 40 °C	Weibull parameter *n* inverse (Eq. 85)	$n_{ref} = 0.6 \pm 0.06$ $a = 332.5 \pm 50.1$ MPa	SigmaPlot 2000 6.00	Pilavtepe-Çelik et al. [89]

For isothermal conditions, Eq. 79 can also be expressed as a function of the pressure applied (Eq. 91)

$$N(P) = \frac{N_0}{1+10^{\Psi}}\left[10^{\left[\Psi-\left(\frac{P}{P_1}\right)^{n_1}\right]}+10^{-\left(\frac{P}{P_2}\right)^{n_1}}\right] \quad (91)$$

Finally, it is important to note that information concerning any of the Weibull HPP secondary models here presented is scarce (Table 7).

Simultaneous Pressure and Temperature Effects on Quasi-Chemical Kinetic Model Parameters

Only Doona et al. [31] have reported secondary inactivation expressions for the quasi-chemical kinetic model. This includes a general inactivation rate constant (μ) for *E. coli* (207–345 MPa, 30–50 °C) as the minimum slope of the process lethality $L(t)$ (Eq. 93). The time at which μ occurs can be defined as t_μ ($t = t_\mu$), thus $L_\mu = L(t_\mu)$, and the initial phase of the HPP for which no microbial inactivation occurs is defined as the "lag time" ($L_0 = 0$; $t = \lambda$). A straight line of $L(t)$ with slope μ can be observed from L_0 to L_μ as in Eq. 93, and the lag time can be obtained by solving for λ, which is a function of the total microbial plate counts (U) determined experimentally as shown in Eq. 92 .

$$\mu = \frac{L_\mu - L_0}{t_\mu - \lambda} \quad (92)$$

$$L(t) = \frac{d\log_{10}(U(t))}{dt} \quad (93)$$
$$U(t) = M^* + M^{**}$$

$$\mu = \frac{L_\mu - L_0}{t_\mu - \lambda} \quad (94)$$

The pressure dependence of the inactivation rate μ for *E. coli* under isothermal conditions (30–50 °C) showed a log-linear relationship. Furthermore, Doona et al. [31] fitted the experimental data to Eq. 94 to describe the pressure–temperature effect on the kinetic constant $\mu(P, T)$. The coefficient values $C_0 = 4.496 \pm 0.2007$, $C_T = -0.0416 \pm 0.0038$, and $C_P = -0.0417 \pm 0.0028$ are valid only when pressure is expressed in *psi* units, but the model behavior was acceptable in the entire experimental range as observed in Fig. 8a ($R^2 = 0.956$).

$$-\log_{10}\mu(P,T) = C_0 + C_T \cdot T + C_P \cdot P \quad (95)$$

The application of this secondary model was extended to predict the time (t_p) required for 6 decimal reductions in *E. coli* counts for various pressure and temperature combinations. The extended model (Eq. 95) also included the lag time (λ), and the predicted processing times to achieve log $N/N_0 = -6$ (t_p) were consistent with a new set of experimental conditions that were selected for validation (Fig. 8b).

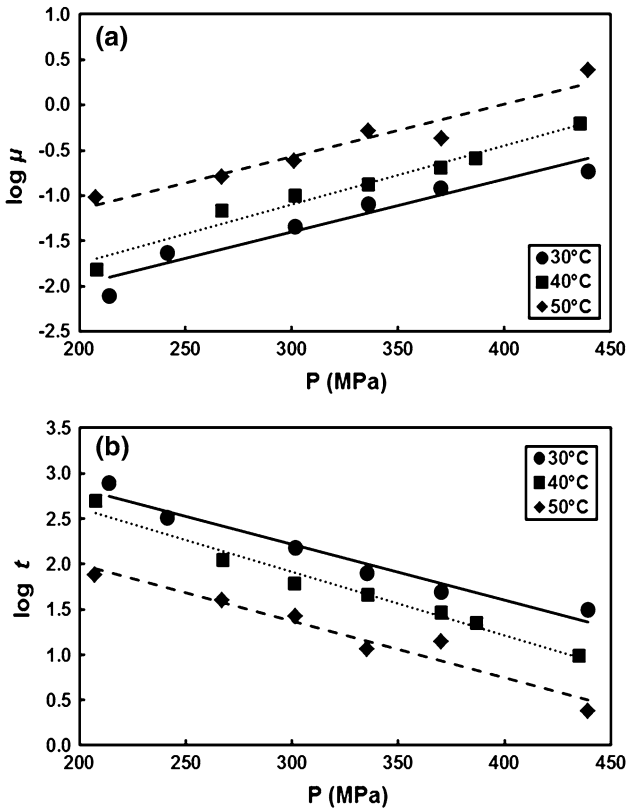

Fig. 8 Experimental (*symbols*) and predicted (*lines*) parameters of the quasi-chemical kinetic model (QCKM) for *E. coli* inactivation at different pressure–temperature combinations: **a** inactivation rate constants (μ); **b** PATP times required to yield a 6-log reduction in *E. coli*, modified from Doona et al. [31]

$$t_P = \lambda + \frac{6}{\mu(P,T)} \quad (96)$$

Secondary models for the enhanced quasi-chemical kinetic model (EQCKM) were semiempirical equations based on the Eyring and Arrhenius model, which were discussed in the section describing the EQCKM model.

Simultaneous Pressure and Temperature Effects on Kinetics Models Under Dynamic Conditions

During PATP, the difference in thermophysical and transport properties, and several PATP design variables (inlet fluid, vessel design, location of food samples in the pressure chamber, food product composition, and geometry) affect temperature, leading to heat transfer between the food, pressurizing fluid, vessel walls, and equipment surroundings [5, 28, 40, 41, 50, 54, 76]. Therefore, isothermal conditions are difficult to achieve even for laboratory-scale PATP units, influencing the interpretation and validity of experimental observations. Experimental practices to approach quasi-adiabatic PATP conditions include

(a) isolate the sample and pressurizing fluid in a carrier with low thermal conductivity [26, 27, 37, 92, 102, 115, 119]; (b) reduce the pressurization rate allowing more time to dissipate adiabatic heating; (c) start the kinetic study after thermal equilibrium is achieved [36, 66, 114, 118]; and (d) use dynamic kinetics modeling techniques to interpret the data [60, 64, 87]. However, these experimental approaches do not solve the need to incorporate the dynamic temperature conditions in the design of PATP process meeting desired safety and quality objectives. Therefore, fluid dynamics simulation under PATP conditions *is a must* and numerous authors have made important contributions in this field. However, an in-depth coverage of studies also is beyond the scope of the current review, thus just a few examples will be examined next.

Dynamic Eyring–Arrhenius Model

Ludikhuyze et al. [64] demonstrated that nonisobaric and nonisothermal conditions affected the predicted values of *Bacillus subtilis* α-amylase inactivation in Tris–HCl buffer (0.01 M, pH 8.6) and in a buffer–water–glycerol (15 % w/w) mix. A secondary model that described the pressure and temperature dependence of the first-order kinetics rate constant (k) was previously obtained under uniform pressure–temperature conditions (Eq. 96) and tested for dynamic PATP treatments (Eq. 97) [65]. The secondary inactivation model developed under static pressure–temperature conditions clearly underestimated dynamic P–T effects and Eq. 96 parameters had to be recalculated. A new set of secondary model parameters was obtained by coupling residual activity with the corresponding pressure–temperature profiles, accurately predicting α-amylase inactivation for both static and dynamic PATP conditions ($R^2 = 0.95$–0.98). Additionally, the authors attempted to obtain a model combining both static and dynamic enzymatic kinetic data, although the predictions registered an error between 5 % and over 100 % [64]. Likewise, Ludikhuyze et al. [60] came upon the same situation when validating another empirical secondary model (Eq. 55) for soybean lipoxygenase (LOX) inactivation at 0.1–650 MPa, 10–64 °C).

$$k(P,T) = k_0 \cdot \exp\left\{-\left[B \cdot \left(\frac{1}{T} - \frac{1}{T_0}\right) + C \cdot (P - P_0)\right]\right\} \tag{97}$$

$$\ln\frac{A}{A_0} = \int_0^t k(P,T) \cdot \mathrm{d}t \tag{98}$$

3-Endpoints Method

Envisioning PATP inactivation kinetics as a purely dynamic thermal process based on the 3-endpoints method was recently proposed by Peleg et al. [87]. Measuring microbial counts and other intrinsic properties without interrupting the food treatment is not always possible. For example, a multiple vessel system run, or multiple runs with various holding times when using a single vessel system, is required to determine the kinetic effects of HPP treatments. In the case of thermal treatments, the capillary method cannot be applied for solid food matrixes and the withdrawal of samples is practically impossible [23, 87]. The 3-endpoints method allows the estimation of inactivation model parameters using the final survival ratios ($\log_{10}S$) and their respective temperature profiles [23]. A dynamic Weibull model $\log S[T(t)]$ (Eq. 98) can be obtained as described in the following paragraphs [85, 86].

$$\frac{d\log_{10}S(t)}{\mathrm{d}t} = -b'[T(t)] \cdot n[T(t)] \cdot \left\{-\frac{\log_{10}S(t)}{b'[T(t)]}\right\}^{\frac{n[T(t)]-1}{n[T(t)]}} \tag{99}$$

An equation describing the dynamic changes in the microbial population ($S = \log N/N_0$) can be obtained by calculating the derivative of the Weibull kinetic model (Eq. 9). The process temperature can briefly be assumed to remain constant at $t = t^*$ (Eqs. 99–100). Thus, the slope at $t = t^*$ is equal to the instantaneous surviving population (Fig. 9), and by substituting Eq. 100 in Eq. 99, the dynamic Weibull kinetic model is obtained (Eq. 98).

$$\left|\frac{d\log_{10}S(t)}{\mathrm{d}t}\right|_T = -b'(T) \cdot n(T) \cdot t^{n(T)-1} \tag{100}$$

$$t* = \left\{-\frac{\log_{10}S(t)}{b[T(t)]}\right\}^{\frac{1}{n(t)}} \tag{101}$$

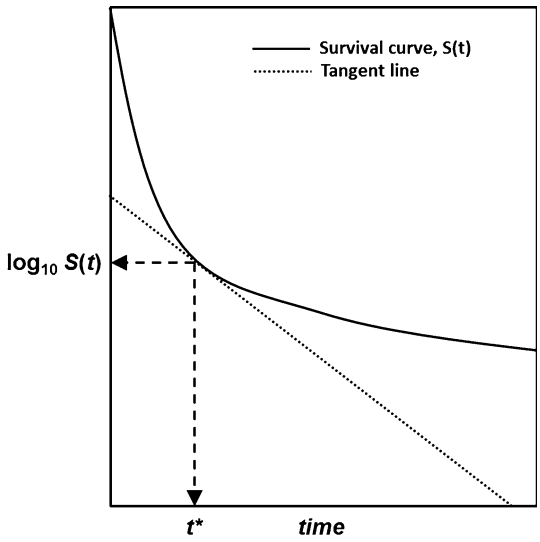

Fig. 9 Instantaneous microbial survival rate (Eq. 100) predicted by the dynamic Weibull inactivation model (Eq. 98), modified from Peleg et al. [85]

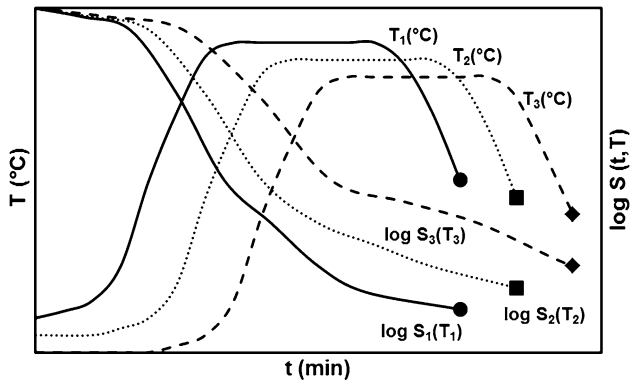

Fig. 10 Schematic example of the HPP temperature profiles and population survival parameters required for the 3-endpoint method, modified from Peleg et al. [87]

The logistic model for b' (T) described by Eq. 79 was incorporated in the dynamic Weibull model (Eq. 98) by Peleg et al. [87]. If temperature has no effect on the shape parameter n, three final survival ratios (S_1, S_2, and S_3) and three temperature profiles (T_1, T_2, and T_3) are needed (Fig. 10) to formulate a 3 × 3 differential equation system whose solution will yield the dynamic Weibull model parameters n, w_c, and T_c [23]. However, Peleg et al. [87] highlighted the model impracticality when the pressure dependence of b' is incorporated (Eq. 80) and the difficulties to numerically solve the differential equation system when n can no longer be considered constant in the temperature and pressure range of interest.

Final Remarks

At present, the availability of kinetics model and data for the pressure processing of foods is still very limiting, inconsistent, and lagging behind the standardized information available for food pasteurization and sterilization by conventional thermal treatments. Parameters describing the microbial inactivation kinetics have been determined mostly only for the primary models most frequently utilized in thermal food processing, i.e., first-order kinetics, Weibull, and log-logistic models, whereas the Bigelow model is still the only one generally used for secondary modeling. Applications of nonlinear models such as the Weibull and log-logistic equations, frequently used to describe the nonlinear behavior observed typically in the pressure inactivation of enzymes, were not found.

Although a large number of empirical and phenomenological secondary models predicting pressure and temperature effects on the inactivation rate constant for the pressure inactivation of enzymes and microorganisms were found and are presented in this review, no general model has been developed. This may reflect the complexity of the kinetics of inactivation by pressure and the insufficiency of good-quality experimental data. Since narrow experimental ranges were consistently observed in the literature reviewed, extreme caution is recommended. The limited number of experimental conditions considered in these experiments may lead to the misinterpretation of results. Thus, kinetic studies covering 600 MPa pressure and 50 °C temperature intervals, respectively, appear sufficient when evaluating the inactivation kinetics of most moderate- and high-pressure/temperature-resistant microorganisms and enzymes. Moreover, the increasing availability of mathematical tools, computer software, and high-pressure equipment instrumentation has motivated researchers to increase the amount of dynamic kinetic model data since knowledge of the temperature gradients generated within the vessel is crucial for the assessment of PATP/PATS applications.

Acknowledgments The authors acknowledge the support from the Tecnológico de Monterrey (Research Chair Funds CAT-200 and Nutrigenomica), México's CONACYT Scholarship Program, and Formula Grants No. 2011-31200-06041 and 2012-31200-06041 from the USDA National Institute of Food and Agriculture.

References

1. Ahn J, Balasubramaniam VM, Yousef AE (2007) Inactivation kinetics of selected aerobic and anaerobic bacterial spores by pressure-assisted thermal processing. Int J Food Microbiol 113(3):321–329
2. Atkins P, de Paula J (2006) Atkins' physical chemistry, 8th edn. Oxford University Press, Oxford, Great Britain
3. Balasubramaniam VM, Farkas DF, Turek E (2008) Preserving foods through high-pressure processing. Food Technol 62(11):32–38
4. Baranyi J, Roberts TA (1994) A dynamic approach to predicting bacterial growth in food. Int J Food Microbiol 23(3–4):277–294
5. Barbosa-Cánovas GV, Juliano P (2008) Food sterilization by combining high pressure and thermal energy. In: Gutiérrez-López GF, Barbosa-Cánovas GV, Welti-Chanes J, Parada-Arias E (eds) Food engineering: integrated approaches. Springer, New York, pp 9–46
6. Basak S, Ramaswamy HS, Simpson BK (2001) High pressure inactivation of pectin methyl esterase in orange juice using combination treatments. J Food Biochem 25:509–526
7. Bermúdez-Aguirre D, Barbosa-Cánovas G (2011) An update on high hydrostatic pressure, from the laboratory to industrial applications. Food Eng Rev 3(1):44–61
8. Bigelow WD (1921) The logarithmic nature of thermal death time curves. J Infect Dis 29(5):528–536
9. Borda D, Van Loey A, Smout C, Hendrickx M (2004) Mathematical models for combined high pressure and thermal plasmin inactivation kinetics in two model systems. J Dairy Sci 87(12):4042–4049
10. Buzrul S, Alpas H (2004) Modeling the synergistic effect of high pressure and heat on inactivation kinetics of *Listeria innocua*: a preliminary study. FEMS Microbiol Lett 238(1):29–36
11. Buzrul S, Alpas H, Largeteau A, Demazeau G (2008) Modeling high pressure inactivation of *Escherichia coli* and *Listeria innocua* in whole milk. Eur Food Res Technol 227(2):443–448

12. Campanella OH, Peleg M (2001) Theoretical comparison of a new and the traditional method to calculate *Clostridium botulinum* survival during thermal inactivation. J Sci Food Agric 81(11):1069–1076
13. Carreño J, Gurrea M, Sampedro F, Carbonell J (2011) Effect of high hydrostatic pressure and high-pressure homogenisation on *Lactobacillus plantarum* inactivation kinetics and quality parameters of mandarin juice. Eur Food Res Technol 232(2): 265–274
14. Chen CS, Wu MC (1998) Kinetic models for thermal inactivation of multiple pectinesterases in citrus juices. J Food Sci 63(5):747–750
15. Chen H, Hoover DG (2003) Pressure inactivation kinetics of *Yersinia enterocolitica* ATCC 35669. Int J Food Microbiol 87(1–2):161–171
16. Chen H, Hoover DG (2003) Pressure inactivation kinetics of *Yersinia enterocolitica* ATCC 35669. Int J Food Microbiol 87(1–2):161–171
17. Chen H (2007) Use of linear, Weibull, and log-logistic functions to model pressure inactivation of seven foodborne pathogens in milk. Food Microbiol 24(3):197–204
18. Clark NA (1979) Thermodynamics of the re-entrant nematic-bilayer smectic a transition. J Phys Colloq 40(C3):C3-345–C343-349
19. Cole MB, Davies KW, Munro G, Holyoak CD, Kilsby DC (1993) A vitalistic model to describe the thermal inactivation of *Listeria monocytogenes*. J Ind Microbiol Biotechnol 12(3):232–239
20. Cook DW (2003) Sensitivity of vibrio species in phosphate-buffered saline and in oysters to high-pressure processing. J Food Prot 66(12):2276–2282
21. Coroller L, Leguerinel I, Mettler E, Savy N, Mafart P (2006) General model, based on two mixed Weibull distributions of bacterial resistance, for describing various shapes of inactivation curves. Appl Environ Microbiol 72(10):6493–6502
22. Corradini MG, Normand MD, Peleg M (2005) Calculating the efficacy of heat sterilization processes. J Food Eng 67(1–2):59–69
23. Corradini MG, Normand MD, Newcomer C, Schaffner DW, Peleg M (2009) Extracting survival parameters from isothermal, isobaric, and "iso-concentration" inactivation experiments by the "3 end points method". J Food Sci 74(1):R1–R11
24. Cruz RMS, Rubilar JF, Ulloa PA, Torres JA, Vieira MC (2011) New food processing technologies: development and impact on the consumer acceptability. In: Columbus F (ed) Food quality: control, analysis and consumer concerns. Nova Science Publishers, New York, NY, pp 555–584
25. Daek T, Farkas J (2012) Thermal destruction of microorganisms. In: Microbiology of thermally preserved foods: canning and novel physical methods. DEStech Publications, Inc., Lancaster, PA, pp 105–160
26. Daryaei H, Balasubramaniam VM (2013) Kinetics of *Bacillus coagulans* spore inactivation in tomato juice by combined pressure–heat treatment. Food Control 30(1):168–175
27. de Heij W, van Scepdael L, Moezelaar R, Hoogland H, Master AM, Van den Berg RW (2003) High-pressure sterilization: maximizing the benefits of adiabatic heating. Food Technol 57(3):37–41
28. Denys S, Van Loey AM, Hendrickx ME (2000) A modeling approach for evaluating process uniformity during batch high hydrostatic pressure processing: combination of a numerical heat transfer model and enzyme inactivation kinetics. Innov Food Sci Emerg Technol 1(1):5–19
29. Dogan C, Erkmen O (2004) High pressure inactivation kinetics of *Listeria monocytogenes* inactivation in broth, milk, and peach and orange juices. J Food Eng 62(1):47–52
30. Doona CJ, Feeherry FE, Ross EW (2005) A quasi-chemical model for the growth and death of microorganisms in foods by non-thermal and high-pressure processing. Int J Food Microbiol 100(1–3):21–32
31. Doona CJ, Feeherry FE, Ross EW, Corradini M, Peleg M, (2008) The Quasi-chemical and Weibull distribution models of nonlinear inactivation kinetics of *Escherichia Coli* ATCC 11229 by high pressure processing. High Pressure Processing of Foods. Blackwell Publishing Ltd, pp 115–144
32. Doona CJ, Feeherry FE, Ross EW, Kustin K (2012) Inactivation kinetics of *Listeria monocytogenes* by high-pressure processing: pressure and temperature variation. J Food Sci 77(8):M458–M465
33. Eisenmenger MJ, Reyes-De-Corcuera JI (2009) High pressure enhancement of enzymes: a review. Enzyme Microb Technol 45(5):331–347
34. Fachin D, Loey AV, VanLoeyIndrawati A, Ludikhuyze L, Hendrickx M (2002) Thermal and high-pressure inactivation of tomato polygalacturonase: a kinetic study. J Food Sci 67(5):1610–1615
35. Farkas DF, Hoover DG (2000) High pressure processing. J Food Saf 65:47–64
36. Ghawi SK, Methven L, Rastall RA, Niranjan K (2012) Thermal and high hydrostatic pressure inactivation of myrosinase from green cabbage: a kinetic study. Food Chem 131(4):1240–1247
37. Grauwet T, Plancken IVD, Vervoort L, Hendrickx ME, Loey AV (2010) Protein-based indicator system for detection of temperature differences in high pressure high temperature processing. Food Res Int 43(3):862–871
38. Guan D, Chen H, Hoover DG (2005) Inactivation of *Salmonella typhimurium* DT 104 in UHT whole milk by high hydrostatic pressure. Int J Food Microbiol 104(2):145–153
39. Guan D, Chen H, Ting EY, Hoover DG (2006) Inactivation of *Staphylococcus aureus* and *Escherichia coli* O157: H7 under isothermal-endpoint pressure conditions. J Food Eng 77(3):620–627
40. Hartmann C, Delgado A (2002) Numerical simulation of convective and diffusive transport effects on a high-pressure-induced inactivation process. Biotechnol Bioeng 79(1):94–104
41. Hartmann C, Delgado A (2003) The influence of transport phenomena during high-pressure processing of packed food on the uniformity of enzyme inactivation. Biotechnol Bioeng 82(6):725–735
42. Hashizume C, Kimura K, Hayashi R (1995) Kinetic analysis of yeast inactivation by high pressure treatment at low temperatures. Biosci Biotechnol Biochem 59(8):1455–1458
43. Hawley SA (1971) Reversible pressure-temperature denaturation of chymotrypsinogen. Biochemistry 10(13):2436–2442
44. Heremans K (1982) High pressure effects on proteins and other biomolecules. Annu Rev Biophys Bioeng 11(1):1–21
45. Heremans K, Smeller L (1998) Protein structure and dynamics at high pressure. Biochim Biophys Acta (BBA) Protein Struct Mol Enzymol 1386(2):353–370
46. Holdsworth D, Simpson R (2007) Kinetics of thermal processing. In: Thermal processing of packaged foods. Springer, US, pp 87–122
47. House JE (2007) Techniques and methods. In: House JE (ed) Principles of chemical kinetics, 2nd edn. Elsevier Academic Press, Burlington, MA, pp 79–109
48. Indrawati I, Van Loey AM, Ludikhuyze LR, Hendrickx ME (1999) Soybean lipoxygenase inactivation by pressure at subzero and elevated temperatures. J Agric Food Chem 47(6):2468–2474
49. Indrawati I, Van Loey A, Ludikhuyze L, Hendrickx M (2001) Pressure-temperature inactivation of lipoxygenase in green peas (*Pisum sativum*): a kinetic study. J Food Sci 66(5):686–693
50. Infante JA, Ivorra B, Ramos ÁM, Rey JM (2009) On the modelling and simulation of high pressure processes and inactivation of enzymes in food engineering. Math Models Methods Appl Sci 19(12):2203–2229
51. Isaacs NS (1981) Effects of pressure on rate processes. In: Isaacs NS (ed) Liquid phase high pressure chemistry, 1st edn. John Wiley & Sons Inc., Toronto, pp 181–352
52. Katsaros GI, Tsevdou M, Panagiotou T, Taoukis PS (2010) Kinetic study of high pressure microbial and enzyme

inactivation and selection of pasteurisation conditions for Valencia Orange Juice. Int J Food Sci Technol 45(6):1119–1129
53. Kingsley DH, Holliman DR, Calci KR, Chen H, Flick GJ (2007) Inactivation of a norovirus by high-pressure processing. Appl Environ Microbiol 73(2):581–585
54. Knoerzer K, Juliano P, Roupas P, Versteeg C (2011) Innovative food processing technologies: advances in multiphysics simulation. Blackwell Publishing Ltd, Hoboken, NJ
55. Koo J, Jahncke ML, Reno PW, Hu X, Mallikarjunan P (2006) Inactivation of *Vibrio parahaemolyticus* and *Vibrio vulnificus* in phosphate-buffered saline and in inoculated whole oysters by high-pressure processing. J Food Prot 69(3):596–601
56. Koseki S, Yamamoto K (2007) A novel approach to predicting microbial inactivation kinetics during high pressure processing. Int J Food Microbiol 116(2):275–282
57. Lado BH, Yousef AE (2002) Alternative food-preservation technologies: efficacy and mechanisms. Microbes Infect 4:433–440
58. Leskovac V (2003) Chemical kinetics. In: Comprehensive enzyme kinetics. Kluwer Academic/Plenum Publishers, New York, NY, pp 11–30
59. López-Gómez A, Fernández P, Palop A, Periago P, Martinez-López A, Marin-Iniesta F, Barbosa-Cánovas G (2009) Food safety engineering: an emergent perspective. Food Eng Rev 1(1):84–104
60. Ludikhuyze L, Indrawati I, Van den Broeck I, Weemaes C, Hendrickx M (1998) Effect of combined pressure and temperature on soybean lipoxygenase. 2. Modeling inactivation kinetics under static and dynamic conditions. J Agric Food Chem 46(10):4081–4086
61. Ludikhuyze L, Indrawati I, Van den Broeck I, Weemaes C, Hendrickx M (1998) Effect of combined pressure and temperature on soybean lipoxygenase. 1. Influence of extrinsic and intrinsic factors on isobaric-isothermal inactivation kinetics. J Agric Food Chem 46(10):4074–4080
62. Ludikhuyze L, Claeys W, Hendrickx M (2000) Combined pressure—temperature inactivation of alkaline phosphatase in bovine milk: a kinetic study. J Food Sci 65(1):155–160
63. Ludikhuyze L, Loey A, Denys IS, Hendrickx MEG (2002) Effects of high pressure on enzymes related to food quality. In: Hendrickx MEG, Knorr D, Ludikhuyze L, Loey A, Heinz V (eds) Ultra high pressure treatments of foods. Springer, US, pp 115–166
64. Ludikhuyze LR, Van den Broeck I, Weemaes CA, Hendrickx ME (1997) Kinetic parameters for pressure − temperature inactivation of *Bacillus subtilis* α-amylase under dynamic conditions. Biotechnol Prog 13(5):617–623
65. Ludikhuyze LR, Van den Broeck I, Weemaes CA, Herremans CH, Van Impe JF, Hendrickx ME, Tobback PP (1997) Kinetics for isobaric-isothermal inactivation of *Bacillus subtilis* α-amylase. Biotechnol Prog 13(5):532–538
66. Ly-Nguyen B, Van Loey AM, Smout C, ErenÖzcan S, Fachin D, Verlent I, Truong SV, Duvetter T, Hendrickx ME (2003) Mild-heat and high-pressure inactivation of carrot pectin methylesterase: a kinetic study. J Food Sci 68(4):1377–1383
67. Mafart P, Couvert O, Gaillard S, Leguerinel I (2002) On calculating sterility in thermal preservation methods: application of the Weibull frequency distribution model. Int J Food Microbiol 72(1–2):107–113
68. Mañas P, Pagán R (2005) Microbial inactivation by new technologies of food preservation. J Appl Microbiol 98(6):1387–1399
69. Meersman F, Smeller L, Heremans K (2006) Protein stability and dynamics in the pressure–temperature plane. Biochim Biophys Acta (BBA) Proteins Proteomics 1764(3):346–354
70. Missen RW, Mims CA, Saville BA (1999). Fundamentals of reaction rates. In: Introduction to chemical reaction engineering and kinetics. John Wiley & Sons, Inc., New York, NY, pp 115–153
71. Morales-Blancas EF, Torres JA (2003a) Thermal resistance constant. In: Heldman DR (ed) Encyclopedia of agricultural, food, and biological engineering. Marcel Dekker, Inc., New York, pp 1030–1037
72. Morales-Blancas EF, Torres JA (2003b). Activation energy in thermal process calculations. In: Heldman DR (ed) Encyclopedia of agricultural, food, and biological engineering. Marcel Dekker, Inc., New York, pp 1–4
73. Morild E (1981) The theory of pressure effects on enzymes. In: Anfinsen CB, Edsall JT, Richards FM (eds) Advances in protein chemistry. Academic Press, London, pp 93–166
74. Mújica-Paz H, Valdez-Fragoso A, Samson C, Welti-Chanes J, Torres J (2011) High-pressure processing technologies for the pasteurization and sterilization of foods. Food Bioprocess Technol 4(6):969–985
75. NCFST (2009) NCFST receives regulatory acceptance of novel food sterilization process. http://www.avure.com/archive/documents/Press-release/ncfst-receives-regulatory-acceptance-of-novel-food-sterilization-process.pdf
76. Otero L, Ramos AM, de Elvira C, Sanz PD (2007) A model to design high-pressure processes towards an uniform temperature distribution. J Food Eng 78(4):1463–1470
77. Otero L, Guignon B, Aparicio C, Sanz PD (2010) Modeling thermophysical properties of food under high pressure. Crit Rev Food Sci Nutr 50(4):344–368
78. Palou E, López-Malo A, Barbosa-Cánovas G, Swanson BG (2007) High-pressure treatment in food preservation. In: Rahman MS (ed) Handbook of food preservation, 2nd edn. CRC Press, Boca Ratón, FL, pp 815–853
79. Parish ME (1998) High pressure inactivation of *Saccharomyces cerevisiae*, endogenous microflora and pectinmethylesterase in orange juice. J Food Saf 18:57–65
80. Patazca E, Koutchma T, Balasubramaniam VM (2007) Quasi-adiabatic temperature increase during high pressure processing of selected foods. J Food Eng 80(1):199–205
81. Patterson MF (2005) Microbiology of pressure-treated foods. J Appl Microbiol 98(6):1400–1409
82. Patterson MF, Linton M (2009) "Pasteurización" de alimentos por altas presiones. In: Nuevas tecnologías en la conservación y transformación de alimentos. International Marketing & Communication, SA, pp 59–72
83. Peleg M, Cole MB (1998) Reinterpretation of microbial survival curves. Crit Rev Food Sci Nutr 38(5):353–380
84. Peleg M, Engel R, Gonzalez-Martinez C, Corradini MG (2002) Non-arrhenius and non-WLF kinetics in food systems. J Sci Food Agric 82(12):1346–1355
85. Peleg M, Normand MD, Corradini MG (2005) Generating microbial survival curves during thermal processing in real time. J Appl Microbiol 98(2):406–417
86. Peleg M (2006) Advanced quantitative microbiology for foods and biosystems. CRC Press, Boca Ratón, FL
87. Peleg M, Corradini MG, Normand MD (2012) On quantifying nonthermal effects on the lethality of pressure-assisted heat preservation processes. J Food Sci 77(1):R47–R56
88. Pérez PMC, Aliaga RD, Reyes SD, López MA (2007) Pressure inactivation kinetics of *Enterobacter sakazakii* in infant formula milk. J Food Prot 70(10):2281–2289
89. Pilavtepe-Çelik M, Buzrul S, Alpas H, Bozoğlu F (2009) Development of a new mathematical model for inactivation of *Escherichia coli* O157: H7 and *Staphylococcus aureus* by high hydrostatic pressure in carrot juice and peptone water. J Food Eng 90(3):388–394
90. Polydera AC, Galanou E, Stoforos NG, Taoukis PS (2004) Inactivation kinetics of pectin methylesterase of greek Navel orange juice as a function of high hydrostatic pressure and temperature process conditions. J Food Eng 62(3):291–298

91. Rajan S, Pandrangi S, Balasubramaniam VM, Yousef AE (2006) Inactivation of *Bacillus stearothermophilus* spores in egg patties by pressure assisted thermal processing. Lebensmittel-Wissenschaft-und-Technologie 39(8):844–851
92. Ramaswamy HS, Shao Y, Zhu S (2010) High-pressure destruction kinetics of *Clostridium sporogenes* ATCC 11437 spores in milk at elevated quasi-isothermal conditions. J Food Eng 96(2):249–257
93. Ramirez R, Saraiva J, Pérez Lamela C, Torres J (2009) Reaction kinetics analysis of chemical changes in pressure-assisted thermal processing. Food Eng Rev 1(1):16–30
94. Ramos ÁM, Smith N (2009) Mathematical models in food Engineering. In: Proceedings of the Conference Name, Conference Location
95. Rauh C, Baars A, Delgado A (2009) Uniformity of enzyme inactivation in a short-time high-pressure process. J Food Eng 91(1):154–163
96. Reineke K, Mathys A, Knorr D (2011) The impact of high pressure and temperature on bacterial spores: inactivation mechanisms of *Bacillus subtilis* above 500 MPa. J Food Sci 76(3):M189–M197
97. Reyns KMFA, Soontjens CCF, Cornelis K, Weemaes CA, Hendrickx ME, Michiels CW (2000) Kinetic analysis and modelling of combined high-pressure–temperature inactivation of the yeast *Zygosaccharomyces bailii*. Int J Food Microbiol 56(2–3):199–210
98. Ross EW, Taub IA, Doona CJ, Feeherry FE, Kustin K (2005) The mathematical properties of the quasi-chemical model for microorganism growth—death kinetics in foods. Int J Food Microbiol 99(2):157–171
99. Santillana Farakos SM, Zwietering MH (2011) Data analysis of the inactivation of foodborne microorganisms under high hydrostatic pressure to establish global kinetic parameters and influencing factors. J Food Prot 74(12):2097–2106
100. Saucedo-Reyes D, Marco-Celdrán A, Pina-Pérez MC, Rodrigo D, Martínez-López A (2009) Modeling survival of high hydrostatic pressure treated stationary- and exponential-phase *Listeria innocua* cells. Innov Food Sci Emerg Technol 10(2):135–141
101. Segovia Bravo K, Ramírez R, Durst R, Escobedo-Avellaneda ZJ, Welti-Chanes J, Sanz PD, Torres JA (2012) Formation risk of toxic and other unwanted compounds in pressure-assisted thermally processed foods. J Food Sci 77(1):1–10
102. Shao Y, Zhu S, Ramaswamy H, Marcotte M (2010) Compression heating and temperature control for high-pressure destruction of bacterial spores: an experimental method for kinetics evaluation. Food Bioprocess Technol 3(1):71–78
103. Smeller L (2002) Pressure–temperature phase diagrams of biomolecules. Biochim Biophys Acta (BBA) Protein Struct Mol Enzymol 1595(1–2):11–29
104. Smith JM, Van Ness HC, Abbot MM (1997) Introducción a la termodinámica en ingeniería químcia, 5th edn. McGraw-Hill/Interamericana, Distrito Federal
105. Toledo RT (2007) Fundamentals of food process engineering, 3rd edn. Springer, Athens
106. Torres JA, Velazquez G (2005) Commercial opportunities and research challenges in the high pressure processing of foods. J Food Eng 67(1–2):95–112
107. Torres JA, Sanz PD, Otero L, Pérez Lamela C, Saldaña MDA (2009) Temperature distribution and chemical reactions in foods treated by pressure-assisted thermal processing. In: Ortega-Rivas E (ed) Processing effects on safety and quality of foods. CRC Taylor & Francis Inc., Boca Raton, pp 415–440
108. Valdez-Fragoso A, Mújica-Paz H, Welti-Chanes J, Torres J (2011) Reaction kinetics at high pressure and temperature: effects on milk flavor volatiles and on chemical compounds with nutritional and safety importance in several foods. Food Bioprocess Technol 4(6):986–995
109. van Asselt ED, Zwietering MH (2006) A systematic approach to determine global thermal inactivation parameters for various food pathogens. Int J Food Microbiol 107(1):73–82
110. van Boekel MAJS (2002) On the use of the Weibull model to describe thermal inactivation of microbial vegetative cells. Int J Food Microbiol 74(1–2):139–159
111. van Boekel MAJS (2008) Kinetic modeling of food quality: a critical review. Compr Rev Food Sci Food Saf 7(1):144–158
112. Van den Broeck I, Ludikhuyze LR, Van Loey AM, Hendrickx ME (2000) Inactivation of orange pectinesterase by combined high-pressure and temperature treatments: a kinetic study. J Agric Food Chem 48(5):1960–1970
113. Van Eldik R, Asano T, Le Noble WJ (1989) Activation and reaction volumes in solution. 2. Chem Rev 89(3):549–688
114. Van Opstal I, Vanmuysen SCM, Wuytack EY, Masschalck B, Michiels CW (2005) Inactivation of *Escherichia coli* by high hydrostatic pressure at different temperatures in buffer and carrot juice. Int J Food Microbiol 98(2):179–191
115. Van Scepdael L, De Heij W, Hoogland H (2004) Method for high pressure preservation. Patent Application Publication, USA, p 26
116. Vega-Gálvez A, Giovagnoli C, Pérez-Won M, Reyes JE, Vergara J, Miranda M, Uribe E, Di Scala K (2012) Application of high hydrostatic pressure to aloe vera (*Aloe barbadensis* Miller) gel: microbial inactivation and evaluation of quality parameters. Innov Food Sci Emerg Technol 13:57–63
117. Velazquez G, Vázquez P, Vázquez M, Torres JA (2005) Avances en el procesado de alimentos por alta presión Ciencia y Tecnología. Alimentaria 4(005):353–367
118. Verlinde PHCJ, Oey I, Deborggraeve WM, Hendrickx ME, Van Loey AM (2009) Mechanism and related kinetics of 5-methyltetrahydrofolic Acid degradation during combined high hydrostatic pressure – thermal treatments. J Agric Food Chem 57(15):6803–6814
119. Wang B-S, Li B-S, Zeng Q-X, Huang J, Ruan Z, Zhu Z-W, Li LIN (2009) Inactivation kinetics and reduction of *Bacillus coagulans* spore by the combination of high pressure and moderate heat. J Food Process Eng 32(5):692–708
120. Weemaes CA, Ludikhuyze LR, Van den Broeck I, Hendrickx ME (1998) Effect of pH on pressure and thermal inactivation of avocado polyphenol oxidase: a kinetic study. J Agric Food Chem 46(7):2785–2792
121. Weemaes CA, Ludikhuyze LR, Van den Broeck I, Hendrickx ME (1998) Kinetics of combined pressure-temperature inactivation of avocado polyphenoloxidase. Biotechnol Bioeng 60(3):292–300
122. Welti-Chanes J, Barbosa-Cánovas G, Aguilera JM (2002) Engineering and food for the 21st century. CRC Press, Boca Ratón, FL
123. Welti-Chanes J, Martín-González F, Guerrero-Beltrán JA, Barbosa-Cánovas G (2006) Water and biological structures at high-pressure. In: Buera MP, Welti-Chanes J, Lillford PJ, Corti HT (eds) Water properties, pharmaceutical, and biological materials. CRC Press, Boca Ratón, FL, pp 205–231
124. Wilson DR, Dabrowski L, Stringer S, Moezelaar R, Brocklehurst TF (2008) High pressure in combination with elevated temperature as a method for the sterilisation of food. Trends Food Sci Technol 19(6):289–299
125. Yaldagard M, Mortazavi SA, Tabatabaie F (2008) The principles of ultra high pressure technology and its application in food processing/preservation: a review of microbiological and quality aspects. Afr J Biotechnol 7(16):2739–2767
126. Zhou L, Zhang Y, Hu X, Liao X, He J (2009) Comparison of the inactivation kinetics of pectin methylesterases from carrot and peach by high-pressure carbon dioxide. Food Chem 115(2):449–455